HHS Public Access

Author manuscript

Immunity. Author manuscript; available in PMC 2019 April 16.

Published in final edited form as:

Immunity. 2018 April 17; 48(4): 716–729.e8. doi:10.1016/j.immuni.2018.03.015.

KLRG1+ Effector CD8+ T Cells Lose KLRG1, Differentiate into All Memory T Cell Lineages, and Convey Enhanced Protective Immunity

Dietmar Herndler-Brandstetter[1,11,13], **Harumichi Ishigame**[1,2,13,*], **Ryo Shinnakasu**[3,4], **Valerie Plajer**[1], **Carmen Stecher**[1], **Jun Zhao**[1,5,6], **Melanie Lietzenmayer**[1], **Lina Kroehling**[1], **Akiko Takumi**[2], **Kohei Kometani**[3,12], **Takeshi Inoue**[4], **Yuval Kluger**[5,6,7], **Susan M. Kaech**[1], **Tomohiro Kurosaki**[3,4], **Takaharu Okada**[2,8,9,*], and **Richard A. Flavell**[1,10,14,*]

[1]Department of Immunobiology, Yale University School of Medicine, New Haven, CT 06520, USA

[2]Laboratory for Tissue Dynamics, RIKEN Center for Integrative Medical Sciences, Yokohama, Kanagawa 230-0045, Japan

[3]Laboratory for Lymphocyte Differentiation, RIKEN Center for Integrative Medical Sciences, Yokohama, Kanagawa 230-0045, Japan

[4]Laboratory of Lymphocyte Differentiation, WPI Immunology Frontier Research Center, Osaka University, Suita, Osaka 565-0871, Japan

[5]Department of Pathology, Yale University School of Medicine, New Haven, CT 06511, USA

[6]Program of Computational Biology and Bioinformatics, Yale University, New Haven, 06520, CT, USA.

[7]Applied Mathematics Program, Yale University, New Haven, 06520, CT, USA.

[8]Precursory Research for Embryonic Science and Technology, Japan Science and Technology Agency, Kawaguchi, Saitama 332-0012, Japan

[9]Graduate School of Medical Life Science, Yokohama City University, Yokohama, Kanagawa 230-0045, Japan.

[10]Howard Hughes Medical Institute, Yale University School of Medicine, New Haven, CT 06520, USA

[11]Present address: Institute of Cancer Research, Medical University of Vienna, Vienna 1090, Austria

[12]Present address: Department of Cellular and Molecular Immunology, Max Planck Institute of Immunobiology and Epigenetics, Freiburg 79108, Germany

[*]Correspondence: harumichi.ishigame@riken.jp (H.I.), takaharu.okada@riken.jp (T.O.), richard.flavell@yale.edu (R.A.F.).

AUTHOR CONTRIBUTIONS

H.I. and R.A.F. initiated the project. D.H.B., H.I., R.S. and T.O. designed the experiments. D.H.B., H.I., R.S., V.P., C.S., M.L. and A.T. performed the experiments. D.H.B., H.I. and T.O. analyzed the data. D.H.B., H.I., J.Z., L.K. and Y.K. performed bioinformatics analysis. S.M.K. provided reagents and contributed to data interpretation. T.I. and T.K. generated *Bach2*^{Flag} mice. K.K. and T.K. provided *Bach2*$^{flox/flox}$ and *Rosa26*^{Bach2} mice. D.H.B., H.I., T.O. and R.A.F. wrote the manuscript.

DECLARATION OF INTERESTS

The authors declare no competing interests.

[13]Co-first author

[14]Lead Contact

SUMMARY

Protective immunity against pathogens depends on the efficient generation of functionally diverse effector and memory T lymphocytes. However, whether plasticity during effector-to-memory $CD8^+$ T cell differentiation affects memory lineage specification and functional versatility remains unclear. Using genetic fate mapping analysis of highly cytotoxic $KLRG1^+$ effector $CD8^+$ T cells, we demonstrated that $KLRG1^+$ cells receiving intermediate amounts of activating and inflammatory signals, downregulated KLRG1 during the contraction phase in a *Bach2*-dependent manner, and differentiated into all memory T cell linages, including CX_3CR1^{int} peripheral memory cells and tissue-resident memory cells. 'ExKLRG1' memory cells retained high cytotoxic and proliferative capacity distinct from other populations, which contributed to effective anti-influenza and anti-tumor immunity. Our work demonstrates that developmental plasticity of $KLRG1^+$ effector $CD8^+$ T cells is important in promoting functionally versatile memory cells and long-term protective immunity.

IN BRIEF

Herndler-Brandstetter et al. demonstrate that $KLRG1^+$ IL-7Rα^+ effector $CD8^+$ T cells downregulate KLRG1 in a *Bach2*-depenent manner and differentiate into long-lived circulating and tissue-resident 'exKLRG1' memory cells. Developmental plasticity of $KLRG1^+$ effector cells therefore drives functional diversity within memory T cell lineages and promotes enhanced anti-influenza and anti-tumor immunity.

GRAPHICAL ABSTRACT

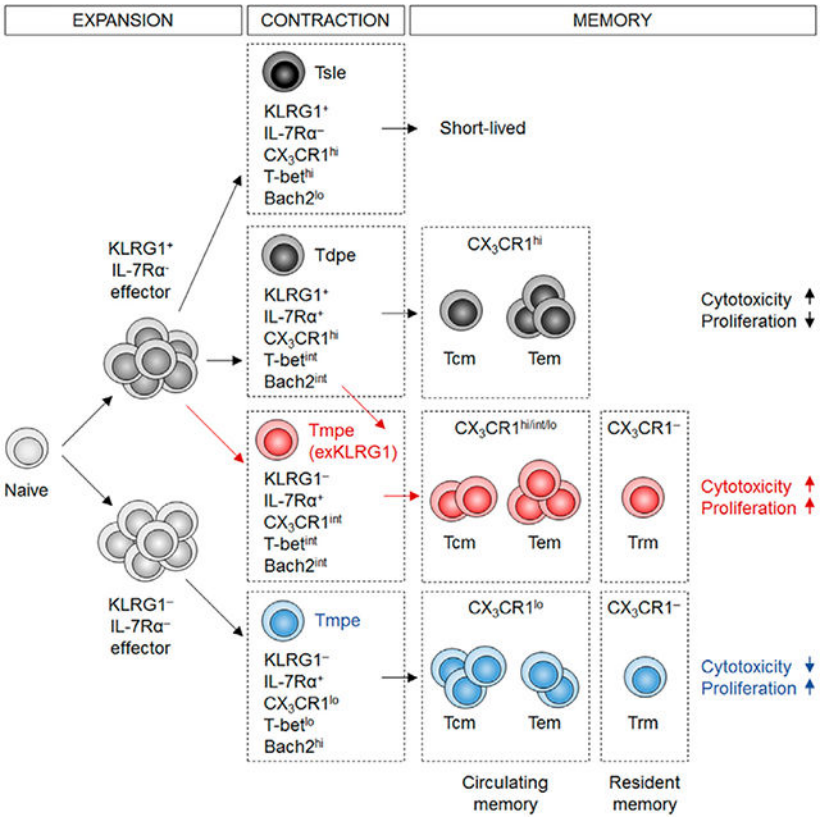

INTRODUCTION

$CD8^+$ T cells are important in host protection from infectious and malignant diseases, and memory $CD8^+$ T cell heterogeneity is a core feature of protective immune responses. Following a primary infection, naïve $CD8^+$ T cells are activated by antigen-presenting cells, clonally expand and differentiate into short-lived effector and long-lived memory cell subsets (Jameson and Masopust, 2009; Mueller et al., 2013; Williams and Bevan, 2007). Two subsets of circulating memory $CD8^+$ T cells with distinct migratory and effector properties have been described: central-memory T (Tcm) and effector-memory T (Tem) cells. Tcm cells express the lymph node (LN) homing receptors CCR7 and CD62L, have a high proliferative capacity but exhibit low cytotoxicity. In contrast, Tem cells lack CCR7 and CD62L, home to non-lymphoid tissues, have a lower proliferative capacity but display high cytotoxicity. In addition, tissue-resident memory T (Trm) cells constitute a recently identified memory cell lineage that does not recirculate but resides in barrier and non-barrier tissues (Mueller et al., 2013; Steinert et al., 2015). Trm cells are phenotypically distinct from recirculating Tcm and Tem cells, and represent the first line of defense upon reinfection at barrier sites, such as the skin and mucosal surfaces. However, considerable heterogeneity within each memory cell lineage has been reported (Kaech and Wherry, 2007; Mackay and Kallies, 2017). For example, a recently identified peripheral memory T (Tpm) cell population, which expresses intermediate levels of CX_3CR1, shares features of both Tcm and Tem cells, and is chiefly responsible for the global surveillance of non-lymphoid tissues

(Gerlach et al., 2016). So far, it remains unclear whether such heterogeneity originates from different effector cell precursors or differential states of activation.

Killer cell lectin-like receptor subfamily G, member 1 (KLRG1) is induced in highly cytotoxic and proliferative effector $CD8^+$ T cells that received strong cumulative T cell receptor and inflammatory signals (Joshi et al., 2007; Sarkar et al., 2008; Xin et al., 2016). KLRG1, together with IL-7Rα, have been used as markers to identify effector $CD8^+$ T cell subsets with distinct traits regarding effector function, migratory properties, long-term survival and multi-lineage memory potential (Buchholz et al., 2016; Chang et al., 2014; Joshi et al., 2007). $KLRG1^+$ IL-$7R\alpha^-$ short-lived effector $CD8^+$ T cells (Tsle) and $KLRG1^+$ IL-$7R\alpha^+$ double-positive effector $CD8^+$ T cells (Tdpe) are thought to have a limited potential to become memory cells, and the $KLRG1^+$ memory $CD8^+$ T cells that develop, gradually decline over time (Joshi et al., 2007; Mackay et al., 2013; Obar and Lefrancois, 2010; Sheridan et al., 2014). In contrast, effector $CD8^+$ T cells that do not express KLRG1 ($KLRG1^-$ IL-$7R\alpha^+$) have been referred to as memory precursor effector cells (Tmpe), which display increased survival during the contraction phase and retain developmental plasticity, as they are able to differentiate into multiple memory cell lineages, including Tcm, Tem and Trm cells (Joshi et al., 2007; Mackay et al., 2013; Obar and Lefrancois, 2010).

The efficient generation of Tmpe cells has been used as an immune parameter critical for long-term protective immunity, in particular at barrier sites (Araki et al., 2009; Mackay et al., 2013; Pearce et al., 2009; Sheridan et al., 2014). However, the expression of proteins such as KLRG1 may not be stable but subject to spatiotemporal regulation by cell-intrinsic and -extrinsic signals (Gerlach et al., 2016; Joshi et al., 2007; Plumlee et al., 2015; Sarkar et al., 2008; Wherry et al., 2003), which may subsequently alter the fate of these effector cells. Whether $KLRG1^+$ effector $CD8^+$ T cell subsets display developmental plasticity, are able to efficiently differentiate into all memory cell lineages, and drive functional heterogeneity among distinct memory cell lineages remains unclear. So far, a fate mapping approach that tracks the fate of different subsets of effector $CD8^+$ T cells in a dynamic and complex *in vivo* setting has not been reported.

In this study, we employed a *Klrg1*^{Cre} reporter system, which enabled longitudinal tracking of $KLRG1^+$ effector $CD8^+$ T cells *in vivo*. By using this system, we demonstrated that $KLRG1^+$ effector $CD8^+$ T cells displayed developmental plasticity, as they were able to downregulate KLRG1 and to efficiently differentiate into all memory T cell lineages. We further showed that such plasticity was a driving force in generating phenotypic and functional diversity within Tcm, Tem and Trm cells. Finally, we showed that exKLRG1 memory cells mounted highly effective anti-influenza and anti-tumor responses, highlighting the functional significance of plasticity in effector-to-memory $CD8^+$ T cell differentiation.

RESULTS

Generation and Validation of *Klrg1*^{Cre} Reporter Mice

To investigate the role of plasticity in effector-to-memory $CD8^+$ T cell differentiation and its impact on memory $CD8^+$ T cell heterogeneity and recall responses, we generated a mouse strain that expressed an eGFP-Cre recombinase (Cre) fusion protein under the control of the

Klrg1 gene (*Klrg1*^{Cre}) (Figure S1A). We then crossed *Klrg1*^{Cre} mice with *Rosa26-flox*-STOP-*flox*-eYFP (*Rosa26*^{eYFP}) or *Rosa26-flox*-STOP-*flox*-tdTomato (*Rosa26*^{tdTomato}) mice. Thus, the fluorescent reporter (eYFP or tdTomato) would permanently tag KLRG1-expressing cells. The analysis of *Klrg1*$^{Cre/+}$*Rosa26* $^{tdTomato/+}$ mice revealed that naïve CD4$^+$ and CD8$^+$ T cells, Gr1$^+$ cells, CD11c$^+$ cells, and CD11b$^+$ cells, which are known not to express KLRG1, did not express the fluorescent reporter (Figure S1B and data not shown). In contrast, cells that frequently express KLRG1, such as NK1.1$^+$ cells, FoxP3$^+$ regulatory T cells and CD8$^+$ Tem cells, expressed the fluorescent reporter (Figures S1B and S1C).

To study the fate of KLRG1$^+$ effector CD8$^+$ T cells during infection *in vivo*, we employed a bacterial (ovalbumin (OVA)-expressing *Listeria monocytogenes*; LM) and a viral (OVA-expressing vesicular stomatitis virus; VSV) infection model (Figures S1D and S1E). Following infection with LM, transferred naïve CD44^{lo} CD62L^{hi} Reporter$^-$ OVA-specific T cell receptor transgenic CD8$^+$ T (OT-I) cells started to upregulate KLRG1 on day 4 p.i., and the vast majority of KLRG1-expressing cells were tagged with the fluorescent reporter (Reporter$^+$ cells) by day 10 p.i. (Figures 1A and S1F). On day 5, the intensity of *Klrg1* and *iCre* mRNA expression correlated with the efficiency of DNA recombination in the *Rosa26* locus (Figure S1G). Cre expression, as determined by fluorescence of eGFP-Cre fusion protein, was restricted to KLRG1^{hi} and KLRG1^{int} effector cells and eGFP-Cre expression was hardly detectable in KLRG1^{lo} effector cells (Figure S1H). The majority of the transferred KLRG1$^+$ Reporter$^-$ effector OT-I cells were also faithfully tagged with the reporter 14 days post transfer (Figure S1I). In addition, both reporter strains (*Klrg1*$^{Cre/Cre}$*Rosa26*$^{eYFP/eYFP}$ and *Klrg1*$^{Cre/+}$*Rosa26*$^{tdTomato/+}$) displayed similar KLRG1 fate mapping efficacy and development of exKLRG1 cells in the blood and spleen (Figures S1J and S1K). Together, these results indicate that KLRG1-expresssing cells are faithfully labeled by the fluorescent reporter once effector CD8$^+$ T cells express sufficient levels of KLRG1.

KLRG1$^+$ Effector CD8$^+$ T Cells Lose KLRG1 Expression and Differentiate into Long-Lived ‘exKLRG1’ Memory Cells

As early as 6 days p.i. with LM, we identified effector OT-I cells in the blood that expressed KLRG1 previously (Reporter$^+$) but lost KLRG1 expression thereafter (Figure 1A). We named this KLRG1$^-$ Reporter$^+$ population ‘exKLRG1’ cells. Following infection with LM, exKLRG1 memory cells survived long-term and represented approximately 25% of the circulating OT-I memory cell pool (Figures 1B and 1C). We also detected long-lived exKLRG1 memory cells in the spleen and LN, where they represented 20% to 35% of the total memory OT-I cell population (Figure 1D). Remarkably, exKLRG1 and KLRG1$^-$ Reporter$^-$ cells had a comparable potential to become long-lived memory CD8$^+$ T cells, as revealed by the fold decrease in cell number between days 10 and 120 p.i. with LM (Figure 1D). Infection with VSV also induced long-lived exKLRG1 memory cells in the blood, spleen and LN (Figures 1E and 1F). Although the intraclonal competition for antigenic and inflammatory signals has been shown to affect the generation of KLRG1$^+$ effector CD8$^+$ T cells, we could detect exKLRG1 memory cells irrespective of the number of naïve OT-I cell precursors transferred (Figures S2A–F). Furthermore, exKLRG1 memory cells also developed from endogenous CD8$^+$ T cells in *Klrg1*$^{Cre/+}$*Rosa26*$^{tdTomato/+}$ mice and

represented 20–40% of the long-lived OVA tetramer$^+$ memory CD8$^+$ T cell population following infection with LM (Figures S2G–J). Together, these results demonstrate that KLRG1$^+$ effector CD8$^+$ T cells are able to differentiate into exKLRG1 memory cells, which represent a significant proportion of the memory cell pool and are able to persist longer than KLRG1$^+$ memory CD8$^+$ T cells. Our results further indicate that a high proportion of cells previously defined as Tmpe cells are actually exKLRG1 cells.

KLRG1$^+$ Effector CD8$^+$ T Cells Downregulate KLRG1 and Differentiate into Trm Cells

Published studies suggest that KLRG1$^-$ Tmpe cells are the predominant effector cell subset able to differentiate into Tcm, Tem and Trm cell lineages, and thereby exhibit multipotency (Mackay et al., 2013; Obar and Lefrancois, 2010; Sheridan et al., 2014). Because our *Klrg1^{Cre}* reporter model allowed us to follow the fate of KLRG1$^+$ effector cells *in vivo*, we re-evaluated whether KLRG1$^+$ effector CD8$^+$ T cells were able to differentiate into Trm cells. Intravenous injection of anti-CD8α phycoerythrin antibody (Anderson et al., 2014) revealed that exKLRG1 memory OT-I cells were able to migrate to the lung parenchyma, while KLRG1$^+$ memory OT-I cells could only be detected in the lung perivascular niche (Figure 2A–2C). In the liver, a preferred site of LM colonization, exKLRG1 and KLRG1$^-$ Reporter$^-$ memory OT-I cells expressed comparable levels of the Trm cell marker CD69 (Figure 2D). The number of exKLRG1 and KLRG1$^-$ Reporter$^-$ Trm cells in the lung and liver was comparable and both liver Trm cell subsets were equally dependent on the survival factor IL-15 (Figure 2C and 2E). Following infection with LM, about 50% of intraepithelial OT-I lymphocytes in the small intestine were exKLRG1 memory cells and KLRG1$^+$ cells were largely excluded from this population (Figure 2F). Oral LM infection also generated exKLRG1 and KLRG1$^-$Reporter$^-$ IELs that expressed the Trm cell markers CD69 and CD103 (Figure 2G), and exKLRG1 cells were enriched within the CD69$^+$ CD103$^-$ cell population (Figure 2H).

Subcutaneous (s.c.) OVA injection of mice that were previously injected with naïve OT-I cells and infected with LM, revealed that up to 40% of OT-I memory cells recruited to the skin epidermis were descendants of KLRG1$^+$ effector cells (Movie S1 and data not shown). Reporter$^+$ Trm cells were also detected in the skin epidermis of uninfected mice following s.c. immunization with OVA plus poly (I:C) (Movie S2 and data not shown). Our results highlight a previously undefined potential of effector CD8$^+$ T cells, which have previously expressed KLRG1, to differentiate into long-lived exKLRG1 Trm cells.

ExKLRG1 Effector CD8$^+$ T Cells Express Key Molecules Associated with Effector Function, Survival, and Proliferation at an Intermediate Level

To better characterize the effector CD8$^+$ T cell subsets that possess developmental plasticity, we first analyzed key molecules and transcription factors in effector cell subsets 8–11 days p.i. with LM. ExKLRG1 effector cells expressed intermediate levels of granzyme B (GzmB), T-bet, Ki-67 and Bcl-2, and similar levels of TCF-1 compared to KLRG1$^-$Reporter$^-$ effector cells (Figure 3A). In addition, exKLRG1 effector cells expressed intermediate levels of *Zeb2*, *Prdm1* and *Bach2* (Figure 3B). The expression level of GzmB, T-bet, Ki-67 and Bcl-2 in exKLRG1 cells was closely associated with the expression levels observed in Tdpe cells (Figure S3A). Following infection with LM, effector CD8$^+$ T cells rapidly up-

regulated CX_3CR1, which is used to identify 3 distinct effector $CD8^+$ T cell subsets with different capacities to generate memory cells (Bottcher et al., 2015; Gerlach et al., 2016), but only $KLRG1^+$ and exKLRG1 cells were able to maintain CX_3CR1 expression during the early memory phase (30 – 60 days p.i.) (Figures 3C and 3D). IL-7Rα expression was downregulated in all effector cell subsets before the peak of expansion (day 5–6 p.i.) (Figure 3C), as reported previously (Joshi et al., 2007; Plumlee et al., 2015; Sarkar et al., 2008). Interestingly, the kinetics of IL-7Rα and CD62L re-acquisition was different among effector T cell subsets (Figures 3C and 3E): $KLRG1^-Reporter^-$ effector cells exhibited the highest degree of IL-7Rα and CD62L re-acquisition, whereas exKLRG1 effector cells re-expressed intermediate levels of these molecules compared to $KLRG1^-Reporter^-$ and $KLRG1^+Reporter^+$ cells (Figures 3C and 3E). Taken together, the development of exKLRG1 memory cells is linked to the degree of effector $CD8^+$ T cell differentiation and proliferative history.

To assess whether phenotypic and functional differences between memory $CD8^+$ T cell subsets correlate with chromatin remodeling early during the effector phase, we analyzed the chromatin accessibility landscape in effector $CD8^+$ T cell subsets using ATAC-seq. The analysis of 7 key loci revealed that exKLRG1 effector cells had an ATAC-seq signal profile that was different from $KLRG1^+Reporter^+$ and $KLRG1^-Reporter^-$ effector cells (Figure 3F). ExKLRG1 effector cells displayed open chromatin states in both effector (*Klrg1*, *Cx3cr1* and *Gzma*) and memory-related gene loci (*Il7r*, *Il2*, *Tcf7* and *Bach2*). Chromatin remodeling in exKLRG1 effector cells may thus explain why exKLRG1 memory cells possess both a high cytotoxic and proliferative capacity.

Tdpe Cells, but not Tsle Cells, Efficiently Give Rise to ExKLRG1 Cells During the Contraction Phase

We next performed a series of effector cell transfer experiments to determine when and which $KLRG1^+$ effector $CD8^+$ T cell subsets differentiated into exKLRG1 memory cells. $KLRG1^+$ $Reporter^+$, $KLRG1^+$ $Reporter^-$, and early $KLRG1^-Reporter^-$ cells (5–6 days p.i. with LM) were all able to differentiate into exKLRG1 cells by day 10–12 p.i. (Figure S4A and S4B) or day 28 p.i. (Figures 4A and 4B). The development of exKLRG1 cells from early $KLRG1^-Reporter^-$ effector cells is explained by previous reports, in which early $KLRG1^-$ effector cells continue to give rise to $KLRG1^+$ cells (Joshi et al., 2007; Plumlee et al., 2015; Sarkar et al., 2008). ExKLRG1 cells descending from early $KLRG1^-Reporter^-$ effector cells expressed intermediate levels of CX_3CR1, IL-7Rα and CD62L compared to $KLRG1^-$ $Reporter^-$ and $KLRG1^+$ $Reporter^+$ cells 12 and 28 days p.i. (Figures S4C and S4D). ExKLRG1 cells derived from $KLRG1^+$ $Reporter^+$ cells, however, displayed higher levels of IL-7Rα and CD62L, and lower levels of CX_3CR1 compared to cells that did not lose KLRG1 12 and 28 days p.i. (Figures S4E and S4F). These results are consistent with our findings of higher IL-7Rα and CD62L, and lower CX_3CR1 expression in exKLRG1 cells than $KLRG1^+$ cells during memory $CD8^+$ T cell differentiation (Figures 3C–3E).

We then isolated $KLRG1^{hi}$ $Reporter^+$ Tsle and Tdpe cells from the spleen of mice 9 days p.i. with LM, and transferred them into infection-matched WT mice (Figures 4C–4F). Thirty-five days p.i., about 15% of Tdpe and 3–5% of Tsle cells had differentiated into exKLRG1

memory cells (Figures 4C and 4D). We also isolated and transferred Reporter$^-$ Tmpe cells, and found that these cells at day 9–11 p.i. displayed a very low potential to develop into exKLRG1 cells (Figures 4C, 4D and S4G) compared to earlier KLRG1$^-$Reporter$^-$ cells. Consistent with the results from day 5–6 early effector cell transfer experiments (Figures S4D and S4F), exKLRG1 cells derived from Tdpe or Tmpe cells expressed intermediate levels of CX_3CR1 and CD62L compared to KLRG1$^+$ and KLRG1$^-$Reporter$^-$ cells (Figures 4E and 4F). A similar number of exKLRG1 and KLRG1$^-$ Reporter$^-$ cells was recovered, while the number of recovered KLRG1$^+$ Reporter$^+$ cells was 6.2 – 9.6 fold lower (Figure S4H). These results are in line with our findings in Figure 1D, and indicate that exKLRG1 and KLRG1$^-$ Reporter$^-$ cells have a similar high potential of survival, while only few KLRG1$^+$ cells survive the contraction phase.

In the absence of antigen, transferred exKLRG1 and KLRG1$^-$ Reporter$^-$ memory cells (day 30 p.i. with LM) did not acquire KLRG1, and KLRG1$^+$ Reporter$^+$ memory cells did not differentiate into exKLRG1 cells (Figure S4I). Together, these results indicate that exKLRG1 cells develop during the late effector and contraction phase, and not during the memory phase, and Tdpe cells represent the preferential effector cell population differentiating into exKLRG1 memory cells.

Molecular Profiling of ExKLRG1 Memory CD8$^+$ T Cells

To determine the lineage relationship of exKLRG1 memory cells, we performed genome-wide transcriptional profiling and compared the transcriptome of exKLRG1 memory OT-I cells with those of KLRG1$^-$ Reporter$^-$ and KLRG1$^+$ memory OT-I cells. Principal component analysis (PCA) revealed that the transcriptome of exKLRG1 memory cells resembled that of KLRG1$^-$Reporter$^-$ memory cells but not KLRG1$^+$ memory cells (Figure S5A). Only 36 genes were differentially expressed (> 1.5-fold) between exKLRG1 and KLRG1$^-$ Reporter$^-$ memory cells, compared to 132 genes differentially expressed between exKLRG1 and KLRG1$^+$ memory cells (Figures S5B and S5C). The analysis of signature genes involved in CD8$^+$ T cell differentiation and function revealed that exKLRG1 memory cells had an intermediate expression level of Tem cell-associated molecules (*Gzma*, *Zeb2*, *Prdm1*, *S1pr5*, *Cx3cr1*, and T-bet) and Tcm cell-associated molecules (*Id3, Socs3*, *Bach2, Myc,* Bcl-2, Eomes, CD62L, CXCR3, CD43, and CCR7) (Figures S5D–S5G) (Best et al., 2013; Bottcher et al., 2015; Dominguez et al., 2015; Xin et al., 2016; Yang et al., 2011). These results indicate that exKLRG1 memory cells are a heterogeneous population consisting of Tcm and Tem cells, whereas KLRG1$^-$Reporter$^-$ or KLRG1$^+$ cells are enriched for Tcm or Tem cells, respectively.

Given the recent report about CX_3CR1^{int} Tpm cells (Gerlach et al., 2016), we analyzed to what extent the characteristics of exKLRG1 memory cells overlapped with those of Tpm cells. We found that exKLRG1 cells in the blood expressed intermediate levels of CX_3CR1 7–60 days p.i. (Figure 3D), and expression of CX_3CR1 was higher in circulating exKLRG1 Tem compared to exKLRG1 Tcm cells (Figure S5H). However, CX_3CR1 expression on exKLRG1 memory cells was decreased by day 299 p.i (Figure 3D). Approximately 42% of CX_3CR1^{int} Tpm cells but only 22–27% of CX_3CR1^{hi} or CX_3CR1^{lo} memory cells were exKLRG1 cells, indicating that CX_3CR1^{int} Tpm cells were enriched in exKLRG1 cells

(Figure S5I). Accordingly, about 70% of KLRG1$^-$ CX$_3$CR1$^+$ but only 27% of KLRG1$^-$ CX$_3$CR1$^-$ memory cells expressed the Reporter (Figure S5J). However, neither exKLRG1 nor KLRG1$^-$ Reporter$^-$ Trm cells in the lung and small intestine expressed CX$_3$CR1 (Figures S5K and S5L). As such, CX$_3$CR1 may be used to distinguish circulating exKLRG1 from KLRG1$^-$ Reporter$^-$ early memory CD8$^+$ T cells.

Functional analysis revealed that exKLRG1 memory cells in the spleen retained a higher cytotoxic capacity compared to KLRG1$^-$ Reporter$^-$ memory cells, as determined by GzmB production (Figure S5M). In contrast, the frequency of IL-2- and IFN-γ-producing cells upon restimulation with OVA peptide *in vitro* was similar between exKLRG1 and KLRG1$^-$ Reporter$^-$ memory CD8$^+$ T cells (Figure S5N and data not shown). These results indicate that exKLRG1 memory cells acquire many features of KLRG1$^-$ Reporter$^-$ memory cells while retaining some characteristics reminiscent of their KLRG1$^+$ effector cell origin.

ExKLRG1 Tcm and Tem Cells Retain High Responsiveness to IL-12

Bystander-mediated activation of memory CD8$^+$ T cells is a key element in the early step of limiting pathogen invasion, and requires responsiveness to inflammatory cytokines but is independent of cognate antigen recognition (Chu et al., 2013; Soudja et al., 2012). We next investigated the responsiveness of exKLRG1 memory cells to inflammatory cytokines (IL-12 alone or in combination with IL-15 or type I interferons (IFN-α/β)) and found that KLRG1$^+$ T cells exhibited the highest cytokine-driven cognate antigen-independent production of IFN-γ compared to KLRG1$^-$ T cell subsets (Figure 5A). Interestingly, a higher percentage of exKLRG1 Tcm and Tem cells produced IFN-γ compared to their corresponding KLRG1$^-$ Reporter$^-$ Tcm and Tem cell counterparts (Figure 5A). Although exKLRG1 cells were enriched in CX$_3$CR1$^+$ cells (Figures 3D and 3E), exKLRG1 cells produced higher amounts of IFN-γ than KLRG1$^-$ Reporter$^-$ cells within the CX$_3$CR1$^+$ or CX$_3$CR1$^-$ population (Figure 5B). The increased cognate antigen-independent production of IFN-γ in exKLRG1 Tem cells was also confirmed *in vivo* by analyzing the recall response to wild-type *Listeria monocytogenes*, which did not express OVA antigen (Figures 5C). However, transferred KLRG1$^+$ and exKLRG1 Tem cells had an equal capacity to expand upon secondary challenge (Figures S5O, right and S5P). Similarly, transferred exKLRG1 and KLRG1$^-$ Reporter$^-$ Tcm cells expanded equally well after re-challenge (Figures S5O, left and S5P). Our results indicate that the responsiveness of Tcm and Tem cells to the inflammatory cytokine IL-12 correlates with their distinct effector cell origin, and the high responsiveness of exKLRG1 memory cells to IL-12 is reminiscent of their KLRG1$^+$ effector cell origin. Yet, the capacity of Tcm and Tem cells to proliferate upon secondary challenge is not affected by their effector cell origin.

ExKLRG1 Trm Cells Retain High Cytotoxic Capacity

We next investigated whether developmental plasticity of KLRG1$^+$ effector CD8$^+$ T cells also generated diversity among Trm cells. We found that the majority of CD69$^+$ Trm cells in the liver expressed high levels of GzmB (Figure 5D). However, a higher frequency of CD69$^+$ exKLRG1 Trm cells expressed GzmB compared to CD69$^+$ KLRG1$^-$ Reporter$^-$ Trm cells (Figure 5E). We next analyzed the Trm cell subsets that were generated in the small intestine epithelium after oral infection with LM (Figure 2H). Both CD103$^+$ and CD103$^-$ exKLRG1

Trm cells in the small intestine epithelium produced more GzmB than their KLRG1^{-} Reporter^{-} Trm cell counterparts (Figure 5F). These results indicate that similar to Tcm and Tem cells, Trm cells display functional diversity, which originates from two different effector cell populations, namely KLRG1^{+} and KLRG1^{-} cells.

ExKLRG1 Memory CD8^{+} T Cells Mount Highly Effective Anti-Viral and Anti-Tumor Responses

We next determined the ability of exKLRG1 memory cells to mediate protective immunity. Although KLRG1^{-} Reporter^{-} cells expanded most efficiently at the site of viral infection (Figure 6A–6B), exKLRG1 and KLRG1^{+} memory cells, but not KLRG1^{-} Reporter^{-} memory cells, provided optimal anti-influenza immunity (Figure 6C). ExKLRG1 cells in the lung quickly re-expressed KLRG1 and upregulated the cytotoxicity marker CD107a to a level comparable to KLRG1^{+} cells (Figures 6D and 6E), indicating that cytolytic activity, rather than recall proliferation, correlated with enhanced protection, which is consistent with published results (Olson et al., 2013). On the other hand, we employed a mouse model of human melanoma, in which Tcm cells with high proliferative capacity drive potent anti-tumor immunity (Klebanoff et al., 2005). KLRG1^{-} Reporter^{-} cells and exKLRG1 cells proliferated and inhibited tumor growth more efficiently than KLRG1^{+} cells (Figures 6F and 6G). These results suggest that the heterogeneous and functionally versatile exKLRG1 memory CD8^{+} T cell population plays an important role in promoting highly effective immune responses in tissues and at barrier sites.

Bach2 Supports ExKLRG1 Memory Cell Development

We then analyzed which factor controlled the differentiation of KLRG1^{+} effector cells into exKLRG1 memory cells. *Bach2* is a transcription repressor that restrains terminal differentiation and supports memory formation of lymphocytes including CD8^{+} T cells and B cells (Hu and Chen, 2013; Roychoudhuri et al., 2016; Shinnakasu et al., 2016). By using *Bach2*^{Flag} reporter mice, we found that Bach2 expression was downregulated in Tsle cells, whereas Tdpe and Tmpe cells retained high expression of Bach2 (Figures S6A–F).

To determine whether *Bach2* is required for the development of exKLRG1 memory cells, we transferred equal numbers of *Klrg1*$^{Cre/+}$*Rosa26*$^{tdTomato/+}$*Bach2*$^{+/+}$ and *Klrg1*$^{Cre/+}$*Rosa26*$^{tdTomato/+}$*Bach*$^{-/-}$ OT-I cells into WT mice and infected them with LM (Figure S7A). As previously reported (Roychoudhuri et al., 2016), *Bach2* deficiency in naïve OT-I cells led to a decrease in the total number of OT-I cells in the blood by day 10 p.i. with LM (Figure S7B). Accordingly, the number of KLRG1^{+}, exKLRG1 and KLRG1^{-} Reporter^{-} cells in the spleen and LN, and the number of exKLRG1 Tcm and exKLRG1 Tem cells in the spleen was significantly reduced on day 27 p.i. in the absence of *Bach2* (Figure 7A and Figure S7C). Importantly, *Bach2* deficiency led to a decreased percentage of exKLRG1 memory cells within Reporter^{+} OT-I cells in the spleen (Figure 7B). Conversely, constitutive expression of *Bach2* in naive OT-I cells by tamoxifen-mediated excision of the STOP cassette in the *Rosa26* locus (*Rosa26*^{Bach2}) (Kuwahara et al., 2016), resulted in considerably impaired expansion of effector CD8^{+} T cells in the spleen and liver on day 10 p.i. with LM (Figures 7C and 7D). *Rosa26*$^{ERT2Cre/Bach2}$ effector OT-I cells exhibited lower Ki-67 expression and retained higher levels of Bcl-2 and CD62L compared with *Rosa26*$^{ERT2Cre/+}$

effector OT-I cells, but failed to express KLRG1 (Figures 7E and S7F). As a result, *Rosa26*$^{ERT2Cre/Bach2}$ memory OT-I cells accumulated in the LN on day 30 p.i. (Figure 7D), indicating that downregulation of Bach2 in naïve CD8$^+$ T cells is essential for the complete differentiation of effector cells.

We next investigated the contribution of Bach2 for the development of exKLRG1 memory cells by crossing *Klrg1*$^{Cre/+}$*Rosa26*$^{tdTomato/+}$ mice with *Bach2*$^{flox/-}$ mice, in order to delete *Bach2* only in effector cells that expressed KLRG1 (Figure S7D). However, we found that the deletion efficiency correlated with the intensity of KLRG1 expression: *Bach2* was efficiently deleted in KLRG1^{hi} cells, but only partially in KLRG1^{int} and exKLRG1 cells (Figures S7E and S7I). Naïve OT-I cells and KLRG1$^-$ Reporter$^-$ memory OT-I cells had the same amount of the *Bach2* floxed allele (Figures S7E and S7F), indicating that *Klrg1*^{Cre}-mediated recombination did not occur in KLRG1$^-$ Reporter$^-$ memory cells. Therefore, we isolated KLRG1^{hi} effector OT-I cells from mice engrafted with *Klrg1*$^{Cre/+}$*Rosa26*$^{tdTomato/+}$*Bach2*$^{+/+}$ or *Klrg1*$^{Cre/+}$*Rosa26*$^{tdTomato/+}$*Bach2*$^{flox/-}$ OT-I cells and transferred them into infection-matched WT mice (Figure 7G). Whereas *Klrg1*$^{Cre/+}$*Rosa26*$^{tdTomato/+}$*Bach2*$^{+/+}$ OT-I cells efficiently differentiated into exKLRG1 cells 22 days post transfer, *Klrg1*$^{Cre/+}$*Rosa26*$^{tdTomato/+}$*Bach2*$^{flox/-}$ OT-I cells were not able to differentiate into exKLRG1 cells (Figure 7H)._Conversely, *Klrg1*^{Cre}-mediated specific induction of *Bach2* in KLRG1$^+$ effector OT-I cells promoted both Tcm and Tem exKLRG1 cell development 10 and 70 days p.i. with LM (Figures 7I–7K). The downregulation of Bach2 was regulated by an AKT-mTOR-Foxo1 pathway (Figures S7G–S7J), and inhibition of this pathway by Rapamycin (Araki et al., 2009) enhanced the conversion of KLRG1$^+$ effector cells into exKLRG1 cells (Figures S7K–S7M). These findings suggest that *Bach2* expressed in Tdpe and Tmpe cells plays an important role in the development of exKLRG1 memory cells.

DISCUSSION

By using a *Klrg1*^{Cre} reporter system, we demonstrate that KLRG1$^+$ IL-7Rα$^+$ effector CD8$^+$ T cells, which receive intermediate levels of activating and inflammatory signals, possess developmental plasticity, as they downregulate KLRG1 during the contraction phase, and enter the pool of long-lived KLRG1$^-$ IL-7Rα$^+$ memory cells. The downregulation of KLRG1 in effector cells is not a singular, stand-alone event, but enables the development of exKLRG1 memory cells, which have a distinct molecular and functional profile, and promote long-lasting protective immunity in tissues and at barrier sites.

The phenotypic and functional diversity among effector cells is thought to shape memory CD8$^+$ T cell heterogeneity and the graded activity of transcription factors in effector CD8$^+$ T cells has been associated with distinct effector cell traits (Kaech and Cui, 2012). Here we demonstrate that exKLRG1 cells express T-bet, Bach2, Zeb2 and Bcl-2 at an intermediate level compared to KLRG1$^+$ and KLRG1$^-$ Reporter$^-$ cells, indicating that T-bet^{int} Tdpe but not T-bet^{hi} Tsle cells possess developmental plasticity, as confirmed by our adoptive cell transfer experiments. We further show that the different properties of exKLRG1 and KLRG1$^-$ Reporter$^-$ memory cells may be due to differences in chromatin accessibility of key effector-(*Klrg1*, *Cx3cr1* and *Gzma*) and memory-related gene loci (*Il7r*, *Il2*, *Tcf7*, and

Bach2), as has been shown for naïve $CD8^+$ T cells responding to viral infection (Scott-Browne et al., 2016), or for the specification of distinct $CD8^+$ T cell fates (Gray et al., 2017; Yu et al., 2017).

ExKLRG1 memory cells express intermediate levels of CX_3CR1 and CD62L reminiscent of recently identified CX_3CR1^{int} Tpm cells, which are the predominant memory $CD8^+$ T cells surveying non-lymphoid tissues (Gerlach et al., 2016). We show that approximately 40% of CX_3CR1^{int} Tpm cells descend from exKLRG1 cells. However, exKLRG1 cells are also found within the CX_3CR1^- and CX_3CR1^{hi} cell populations, which exhibit characteristics of classical Tcm and Tem cells, respectively. These results indicate that exKLRG1 cells partly overlap with, but are not restricted to the CX_3CR1^{int} Tpm fraction. Consistent with the essential roles of IL-12 and T-bet in the induction of KLRG1 and CX_3CR1 during effector $CD8^+$ T cell differentiation, exKLRG1 Tcm and Tem cells retain higher responsiveness to IL-12, but similar proliferative capacity upon rechallenge, compared to $KLRG1^-$ $Reporter^-$ Tcm and Tem cells. This enhanced antigen-independent response of exKLRG1 memory cells may contribute to early anti-microbial protection meditated by bystander-activated memory $CD8^+$ T cells.

CX_3CR1 expression gradually declines in memory $CD8^+$ T cells, in particular in exKLRG1 Tcm cells. Our results are consistent with previous findings that the frequency of CX_3CR1^{hi} cells is gradually decreased over time and CX_3CR1^{int} Tpm cells progressively convert into CX_3CR1^- cells (Gerlach et al., 2016). Together, these results suggest that CX_3CR1 expression may only be suitable to distinguish early circulating exKLRG1 and $KLRG1^-$ $Reporter^-$ memory cells.

Our results demonstrate that the transcription repressor Bach2 does not only control TCR-driven transcriptional programs during the initial activation of $CD8^+$ T cells to indirectly regulate memory $CD8^+$ T cell development (Hu and Chen, 2013; Roychoudhuri et al., 2016), but also regulates developmental plasticity of $KLRG1^+$ effector cells. Although high expression of Bach2 in our overexpression studies promotes both exKLRG1 Tcm and exKLRG1 Tem cell development, the enhancement of exKLRG1 Tcm cell development appears more pronounced. It is possible that the intermediate expression of Bach2 in exKLRG1 cells may equally promote Tcm and Tem cell differentiation. Alternatively, additional transcriptional regulators could be involved in controlling the differentiation of $KLRG1^+$ effector cells into exKLRG1 Tem cells. In addition to the cell-intrinsic role of Bach2 in effector $CD8^+$ T cell survival (Roychoudhuri et al., 2016), Bach2-mediated induction of CD62L may also enable exKLRG1 cells to access distinct survival niches, such as IL-7-producing cells in lymphoid organs (Hara et al., 2012; Jung et al., 2010).

ExKLRG1 cell development continuously occurred during the late effector and contraction phases, but not during the memory phase. It should be noted that although memory exKLRG1 cell development correlated with IL-7Rα re-acquisition, early exKLRG1 effector cells (day 5–7 p.i.) did not express IL-7Rα, indicating that downregulation of KLRG1 precedes the induction of IL-7Rα at this early time point. The different duration of KLRG1 expression may reflect different signal strength received by effector cells, which contributes to fate decision of $KLRG1^+$ effector cells and may contribute to the functional heterogeneity

within exKLRG1 cells. Noteworthy, the frequency of exKLRG1 memory cells reported in our study may be underestimated, because *Cre*-reporter strains may underreport *Cre* activity. We noticed that in about 5–10% of KLRG1$^+$ effector cells, the expression of KLRG1 may have not been strong enough to drive Reporter expression. In fact, not all KLRG1$^+$ effector cells expressed the eGFP-Cre fusion protein and the efficiency of *Klrg1*^{Cre}-mediated deletion of *Bach2* was dependent on the intensity of KLRG1 expression. Some KLRG1$^-$ Reporter$^-$ memory cells may share the features with exKLRG1 cells and therefore be descendants of effector cells that expressed low or intermediate levels of KLRG1.

As reported previously (Mackay et al., 2013; Sheridan et al., 2014), KLRG1$^+$ cells are excluded from the Trm cell population, and adoptive transfer experiments of KLRG1$^-$ and KLRG1$^+$ effector CD8$^+$ T cells suggest that Trm cells derive from KLRG1$^-$ precursor cells (Mackay et al., 2013). However, temporal, spatial and proportional limitations of adoptive transfer experiments in previous studies may have led to underestimate KLRG1$^+$ effector CD8$^+$ T cell plasticity, and its impact on protective immunity at barrier sites. By using *in vivo* fate mapping, we demonstrate that effector CD8$^+$ T cells that have previously expressed KLRG1 are able to migrate into tissue barrier sites, upregulate markers of tissue residency, and represent up to 50% of the Trm cell pool in the liver, lung, skin, and small intestine. Similar to circulating exKLRG1 memory CD8$^+$ T cells, exKLRG1 Trm cells express higher levels of GzmB compared to KLRG1$^-$ Reporter$^-$ Trm cells. These results indicate that Trm cells with distinct functional characteristics originate from two different effector cell populations, namely from effector cells that have previously expressed KLRG1, and KLRG1$^-$ effector cells, although when and where KLRG1$^+$ effector cells downregulate KLRG1 to become exKLRG1 Trm cells remains unclear. Following oral infection with LM, as much as 70% of CD103$^-$ CD69$^+$ Trm cells in the small intestine epithelium are exKLRG1 cells, suggesting that exKLRG1 and KLRG1$^-$ Reporter$^-$ Trm cells. Because CD103$^-$ and CD103$^+$ Trm cells may be differentially localized (Bergsbaken and Bevan, 2015), it is suggested that exKLRG1 and KLRG1$^-$ Reporter$^-$ Trm cells may, in part, seed distinct niches. In contrast to KLRG1$^+$ memory cells, exKLRG1 memory cells express CXCR3, which has been shown to promote the formation of Trm cells (Fernandez-Ruiz et al., 2016; Shin and Iwasaki, 2012). This may allow exKLRG1 cells to enter the epithelium, gain close contact to IL-15-producing cells at barrier sites, and thereby receive the necessary signals for survival and tissue residency (Mortier et al., 2009).

In summary, we demonstrate that developmental plasticity of KLRG1$^+$ effector CD8$^+$ T cells is a driving force in promoting phenotypic and functional diversity among Tcm, Tem and Trm cells. KLRG1$^-$ IL-7Rα$^+$ Tmpe cells with a multi-lineage memory potential are a heterogeneous population, containing cells with a history of KLRG1 expression. These findings redefine our understanding of effector-to-memory CD8$^+$ T cell differentiation and the generation of functional heterogeneity, and could help facilitate the development of more effective T cell-based therapies and vaccines against malignancies and infectious diseases.

CONTACT FOR REAGENT AND RESOURCE SHARING

Further information and requests for resources and reagents should be directed to and will be fulfilled by the Lead Contact, Richard A. Flavell (richard.flavell@yale.edu).

EXPERIMENTAL MODEL AND SUBJECT DETAILS

Mice

OT-I (Jax 003831), UBC-GFP (Jax 004353), *Rosa26*^{eYFP} (Jax 006148), *Rosa26*^{tdTomato} (Jax 007908) mice were obtained from the Jackson Laboratory and *Rag2*$^{-/-}$ mice (RAGN12) were obtained from Taconic Biosciences. *Bach2*$^{flox/flox}$ and *Rosa26*^{Bach2} mice have been described previously (Kometani et al., 2013; Kuwahara et al., 2016). C57BL/6-Ly5.2/Cr (CD45.1) congenic mice were obtained from the National Cancer Institute. C57BL/6 mice were obtained from the National Cancer Institute, Charles River Laboratories and CLEA Japan. All animal studies were performed in accordance with the guidelines of the Office of Animal Research Support of Yale University and the Animal Experiment Committee of the RIKEN Yokohama Institute.

Generation of *Klrg1*^{Cre} Mice

Klrg1^{Cre} mice were generated with a standard cloning strategy. Homologous arms of the *Klrg1* locus were isolated from genomic DNA by PCR. A 2.5 kb fragment containing exons 4 and 5 was used as the 5' homology region and a 2.7 kb fragment containing 3'UTR was used as the 3' homology region. The homologous arms were cloned into a reporter plasmid containing a Frt-flanked Neomycin resistance gene (Neo), a thymidine kinase, and a fragment encoding an IRES-eGFP-iCre fusion protein. The reporter cassette was introduced immediately after the stop codon to avoid disruption of cis-regulatory elements in the 3′ UTR and the polyadenylation signal. The targeting vector was electroporated into C57BL/6-derived JM8A ES cells. After the selection with G418, correctly targeted clones were identified by PCR. To obtain chimeric mice, correctly targeted ES clones were injected into C57BL/6 blastocysts, which were then implanted into CD1 pseudopregnant foster mothers. Male chimaeras were bred with C57BL/6 to screen for germline transmitted offspring. Germline transmitted mice were bred with FLPo (Jax 011065) mice to remove the Neo gene.

Generation of *Bach2*^{Flag} Mice

To generate *Bach2*^{Flag} mice, homologous arms of the *Bach2* locus were cloned from genomic DNA by PCR. A 6.5 kb fragment was used as the 5' homology region and a 2.5 kb fragment was used as the 3' homology region. The homologous arms were cloned into a reporter plasmid containing a Frt-flanked Neo gene, a diphtheria toxin A (DTA), and a 3×Flag-tag which was inserted after the first methionine. The targeting vector was electroporated into C57BL/6-derived Bruce4 ES cells. After the selection with G418, correctly targeted clones were identified by PCR. The targeted ES clones were injected into blastocysts from BALB/c mice. The obtained chimeric mice were crossed with C57BL/6 mice to obtain germline transmitted animals. To remove the Neo cassette, the mice were further crossed to CAG-Flpe mice (Kanki et al., 2006).

Adoptive Cell Transfer, Infection and Tumor Challenge

Spleen and peripheral LN were isolated from *Klrg1*$^{Cre/+}$*Rosa26*$^{tdTomato/+}$OT-I or *Klrg1*$^{Cre/Cre}$*Rosa26*$^{eYFP/eYFP}$OT-I mice on a *Rag2* sufficient or deficient background. Single cell suspension was generated by mechanical disruption and CD8^{+} T cells were enriched by

using EasySep™ Mouse Naive $CD8^+$ T cell Isolation Kit (STEMCELL Technologies) or a biotinylated antibody cocktail (anti-B220 (RA3–6B2), anti-CD4 (RM4–5), anti-CD11b (M1/70), anti-CD11c (N418), and anti-Gr1 (RB6–8C5) antibodies; BioLegend) and MojoSort™ Streptavidin Nanobeads (BioLegend). Naive $CD44^{lo}$ $CD62L^{hi}$ $CD8^+$ $CD45.1^+$ $Reporter^-$ OT-I cells were further purified by a cell sorter (BD Biosciences). A total of 0.5 – 1×10^5 naïve OT-I cells were transferred into C57BL/6 mice (CD45.2), unless otherwise indicated. One day after adoptive transfer, mice were infected intravenously (i.v.) with 1×10^5 recombinant *Listeria monocytogenes* expressing OVA (LM) (Pope et al., 2001), or 1×10^6 plaque-forming units (PFU) recombinant vesicular stomatitis virus expressing OVA (VSV) (Kim et al., 1999). For oral LM infection, mice were orally infected with 1×10^8 CFU of LM. For tissue imaging, $Klrg1^{Cre/+}Rosa26^{tdTomato/+}$OT-I mice were crossed with UBC-GFP mice to detect transferred OT-I cells. For co-transfer experiments, naive control and *Bach2* gene-manipulated OT-I cells, each with a different congenic marker, were mixed at a 1:1 ratio and transferred into C57BL/6 mice. For the in vivo induction of *Bach2* in naïve $CD8^+$ T cells, OT-I $Rosa26^{ERT2Cre/Bach2}$ mice were administered orally with 2 mg of tamoxifen (Sigma-Aldrich) in sunflower seed oil (Sigma-Aldrich) once daily for four consecutive days, and *Bach2*-expressing GFP^+ naïve OT-I cells were sorted 9 days after the initial treatment. For rapamycin treatment, OT-I-engrafted mice were administered i.p. with 300 μg kg^{-1} of rapamycin (Calbiochem) daily from day 8 to day 19 p.i. with LM.

$CD45.1^+$ effector or memory OT-I cells were enriched from the spleen of LM-infected mice by using a biotin-anti-CD45.1 antibody and Streptavidin MicroBeads (Miltenyi Biotec), and further purified by a cell sorter (BD Biosciences). For effector cell transfer experiments, $2 – 5 \times 10^5$ effector OT-I cells were adoptively transferred into infection-matched WT mice. To determine the ability of exKLRG1 memory cells to mediate secondary responses, 1×10^4 memory OT-I cells were adoptively transferred into naïve WT mice that were infected i.n. with OVA-expressing influenza A/PR8 virus (H1N1; FLU) one day later. The lungs were collected 7–8 days p.i. and the amount of influenza virus RNA was determined by quantitative RT-PCR. For the *in vivo* tumor experiment, naïve WT mice were injected with B16 melanoma expressing OVA (1×10^5 cells) (Falo et al., 1995) intradermally into the flank. Five days later, memory OT-I cell subsets were transferred and the mice immediately immunized with 10 μg of OVA (Worthington Biochemical) and 2 μg of poly(I:C) (GE Healthcare) s.c. into the flank. Tumor growth was monitored by measurement of two perpendicular diameters of the skin tumor (mm^2) by caliper every other day. To generate cognate antigen-independent recall responses, OT-I engrafted mice were reinfected i.v. with 1×10^6 wild-type Listeria (EGD) 90 days after primary LM infection.

Flow Cytometry

Fluorescent dye-labeled antibodies targeting Bcl2 (BCL/10C4), CCR7 (4B12), CD4 (RM4–5), CD8α (53–6.7), CD43 (1B11), CD44 (IM7), CD45.1 (A20), CD45.2 (104), CD62L (MEL-14), CD69 (H1.2F3), CD103 (2E7), CD107a (1D4B), CD127 (A7R34), CXCR3 (173), CX_3CR1 (SA011F11), Eomes (Dan11mag), FLAG (DYKDDDDK) (L5), Foxp3 (FJK-16s), Granzyme B (GB11), IFN-γ (XMG1.2), IL-2 (JES6–5H4), Ki-67 (16A8), KLRG1 (2F1), NK1.1 (PK136), T-bet (4B10), and TCF1 (C63D9) were purchased from BioLegend, Thermo Fisher Scientific, BD Biosciences or Cell Signaling Technology. Rabbit

anti-RFP (600–401-379 or 600–406-379) was purchased from Rockland. OVA-K^b tetramer was from MBL. For intracellular cytokine staining, splenocytes from infected mice were stimulated with SIINFEKL peptide in the presence of Protein Transport Inhibitor (BD Biosciences) or Brefeldin A (Biolegend) for 4–5 hours, followed by fixation and permeabilization according to the manufacturer's instructions (BD Biosciences). T-bet, Eomes, Foxp3, and anti-tdTomato staining were performed by eBioscience™ Foxp3/ Transcription Factor Staining Buffer Set (Thermo Fisher Scientific) according to the manufacturer's instructions. The cells were analyzed on a LSRII or FACSCantoII (BD Biosciences) and data were analyzed using FlowJo software (Tree Star).

Intravascular $CD8^+$ T Cell Staining

Mice were injected i.v. (retro-orbital) with 2 μg of anti-CD8α phycoerythrin antibody diluted in 100 μL of sterile PBS as previously described (Anderson et al., 2014). Mice were euthanized and tissues were collected five minutes after injection of the anti-CD8α antibody.

Isolation of Lymphocytes from Non-Lymphoid Organs

Peripheral blood lymphocytes (PBLs) were isolated from retro-orbital vein of infected mice. Liver and lung cell homogenates were digested for 1 hour at 37°C with digestion buffer (RPMI 1640 + 5% FBS + 100 U/ml DNase I (Sigma-Aldrich) + 0.2 mg/mL Collagenase IV (Sigma-Aldrich)). Liver homogenates were centrifuged at 300 rpm for 3 min to remove hepatocytes, and lung homogenates were run through a 70 μm cell strainer (BD Biosciences). Non-hepatic supernatant and lung lymphocytes were centrifuged at 1500 rpm for 10 min. The cell pellet was resuspended in 1 mL of RPMI 1640 + 5% FBS and mixed with 4 ml of 27.5% OptiPrep (Axis-Shield). To make a gradient, 1 mL of RPMI 1640 was layered on top of the cells, and centrifuged at 2000 rpm for 20 min. Lymphocytes were removed from the interface of the gradient. To isolate intraepithelial lymphocytes (IELs), small intestines were opened longitudinally and washed. Small intestines were then cut into short segments, which were transferred into 50 mL conical tubes, and incubated for 30 min at 37°C with gentle shaking in RPMI 1640 containing 2% FBS, 2 mM EDTA, and 1 mM dithioerythritol. Cell suspensions were passed through a 70 μm cell strainer. The cells were resuspended in 4 mL of 40% Percoll (GE Healthcare), and 4 mL of 80% Percoll was underlayed in a 15 mL conical tube. Percoll gradient separation was performed by centrifugation for 20 min at 600 × g at room temperature. IELs were collected at the interphase of the Percoll gradient. Tumor-infiltrating cell were isolated with mechanical disruption of the tumor through a 70 μm cell strainer and resuspended in 40% Percoll solution (GE Healthcare). Cells were collected from the interface of a 40:80 Percoll gradient after centrifugation at 2000 rpm for 20 min.

Intravital Two-Photon Microscopy

Transferred *Klrg1*$^{Cre/+}$*Rosa26*$^{tdTomato/+}$ UBC-GFP^+ OT-I cells in the foot skin were imaged by an inverted TCS SP8 multiphoton microscope (Leica Microsystems) equipped with an HC FLUOTAR L 25×/0.95 W VISIR objective lens (Leica Microsystems) and four non-descanned Hybrid Detectors (Leica Microsystems). Multiphoton excitation was provided by a Chameleon Vision II Ti:Sapphire laser (Coherent) tuned to 910 nm and a Chameleon Compact OPO-converted Chameleon Ultra II Ti:Sapphire laser (Coherent) tuned to 1110

nm. For image acquisition, 466 μm × 466 μm x–y planes were scanned at a resolution of 0.9 μm per pixel and images of 21–29 x–y planes with 3 μm z spacing were formed after averaging eight video frames for each x–y plane. Three-dimensional stacks were captured every 30 s. Emission signals were separated by a dichroic mirror at 560 nm and then further separated by a dichroic mirror at 495 nm. A 460/50-nm emission filter was used for DAPI and second harmonic generation (SHG), a 525/50-nm emission filter for GFP, and a 585/40-nm emission filter for tdTomato.

Tissue Clearing

Tissue clearing was performed as reported previously (Tainaka et al., 2014). Briefly, small intestines and foot skins were fixed with 4% paraformaldehyde, washed with PBS, and then immersed in Reagent 1 containing 25% urea (Nacalai Tesque), 25% N,N,N',N'-tetrakis(2-hydroxypropyl) ethylenediamine (Tokyo Chemical Industry), and 15% polyethylene glycol mono-p-isooctylphenyl ether/Triton X-100 (Nacalai Tesque). Samples were stored at 4°C in the dark until imaging.

RNA-Seq and Bioinformatics Analysis

Memory OT-I cell subsets were isolated from the spleen 104–110 days p.i. with LM and 70 days p.i. with VSV. Total RNA was extracted from at least 1×10^5 cells derived from 5–8 mice using TRIzol™ reagent (Thermo Fisher Scientific). For OT-I memory cell subsets isolated from LM-infected mice, the DNA library was constructed with a SureSelect Strand-Specific RNA Library Prep for Illumina Multiplexed Sequencing (Agilent) according to manufacturer's instruction. The size range of the resulting DNA library was estimated on a 2100 Bioanalyzer (Agilent). After checking the molar concentration by qPCR using a KAPA Library Quantification Kit (Kapa Biosystems), the DNA library was subjected to sequencing on a HiSeq 1500 sequencer (Illumina) in a 49-bp single read mode. For OT-I memory cell subsets isolated from VSV-infected mice, the DNA library was subjected to sequencing on a HiSeq 2500 sequencer (Illumina) in a 75 bp paired-end read mode.

The raw data were processed with CASAVA 1.8.2 (Illumina) to generate fastq files. The sequence reads were aligned to the *Mus musculus* reference genome (GRCm38/mm10) using TopHat2 version 2.0.8 (Kim et al., 2013). Cufflinks version 2.1.1 (Trapnell et al., 2010) was used to calculate the fragments per kilobase of transcript per million fragments mapped (FPKM). Principal component analysis (PCA) was performed with R (http://www.r-project.org/), and visualization generated with *ggplot2* package (Wickham, 2009). The Venn diagram was generated with *VennDiagram* package (Chen and Boutros, 2011). To identify differentially regulated genes, an absolute 1.5-fold-change difference between any two samples and FDR (Benjamini-Hochberg) ≤ 0.1 was used.

ATAC-Seq

To profile open chromatin, we used the ATAC-seq protocol developed by (Buenrostro et al., 2015). In brief, 5×10^4 naïve and effector (8 days p.i. with LM) OT-I cell subsets from the spleen were sorted, centrifuged in cold PBS buffer for 5 min at 500 g, resuspended in 100 μL cold lysis buffer, and centrifuged immediately for 10 min at 500 g. The nuclei pellets were resuspended in the transposition reaction mix (Nextera DNA Library Preparation Kit,

Illumina) and incubated at 37°C for 30 min. Immediately following transposition, a MinElute PCR Purification Kit (Qiagen) was used to purify DNA. To amplify transposed DNA fragments, PCR with barcoded PCR primers (Buenrostro et al., 2013) and NEBNext High-Fidelity 2x PCR Master Mix (New England Biolabs) was performed. To reduce GC and size bias in PCR, the appropriate number of PCR cycles was determined using qPCR. The amplified library was purified using a MinElute PCR Purification Kit. ATAC-seq libraries were sequenced using Illumina HiSeq2500 (75 bp; paired-end), at an average sequencing depth per sample of 35 million reads.

Raw sequencing reads were first processed with *cutadapt-1.8.3* (Martin, 2011) to trim adapters. Bowtie-2 (Langmead and Salzberg, 2012) was used then to align the trimmed reads to the mouse genome mm10 with default parameters. Duplicated reads were marked and removed from the analysis with Picard MarkDuplicate tool (http://broadinstitute.github.io/picard). Subsequently, BEDTools (Quinlan and Hall, 2010) was used to turn the alignment file to a bed file, which was the input of MACS2 (Zhang et al., 2008) to call peaks and produce BedGraph files. Visualizations of coverage on regions of interest were produced with IGV (Robinson et al., 2011).

Quantitative Reverse Transcription PCR (RT-PCR) Analysis

RNA was reverse transcribed into a single-strand cDNA using SuperScript III Reverse Transcriptase (Thermo Fisher Scientific). Quantitative RT-PCR was performed on a 7500 Fast Real-Time PCR system (Applied Biosystems) or a CFX96 Real-Time System (Bio-Rad) using a SYBR FAST universal qPCR kit (KAPA Biosystems). Expression values were calculated using the comparative threshold cycle method and normalized to mouse *Actb*. Sequence-specific oligonucleotide primers were designed using Primer3Plus software, qPrimerDepot or were described elsewhere (Dominguez et al., 2015; Endrizzi and Jameson, 2003; Pillai et al., 2016). The oligonucleotide sequences are listed in the STAR methods section.

In Vitro Cell Cultures

Naïve $CD8^+$ T cells were isolated from the spleen of C57BL/6J mice and were stimulated with Dynabeads Mouse T-Activator CD3/CD28 (Life Technologies) in the presence of 5 ng/mL of rIL-2 (R&D) for 2 days. Where indicated, 20 ng/mL of rapamycin or 1.0 μM of Foxo1 inhibitor (AS1842856; Calbiochem) was added to culture medium.

For retroviral transduction assay, naïve $CD8^+$ T cells were stimulated as described above for 2 days and were spin-infected with retrovirus produced from pMCs-mock-IRES-GFP vector or pMCs-Foxo1-CA-IRES-GFP vector (Harada et al., 2010). 48 h after transduction, the GFP^+ cells were sorted using a FACSAriaII for quantitative RT-PCR analysis.

For the *in vitro* IFN-γ production assay, splenocytes were stimulated with rIL-12 (Peprotech; 50 ng/mL) in combination with rIL-15 (Peprotech; 50 ng/mL) or rIFN-α/β (PBL Assay Science; 250 units/mL each) for 7 hours in the presence of Protein Transport Inhibitor (BD Biosciences).

Immunoblot Analysis

Cells were sorted and cell extracts were prepared using a Nuclear Extract Kit (Active Motif). The cell lysates were separated on 5–20 % SDS-PAGE and transferred to a PVDF membrane (Merck). The membrane was immunoblotted with anti-Bach2 (ab83364, Abcam), anti-FLAG (M2, Sigma-Aldrich), and anti-Actin (C-11, Santa Cruz Biotechnology). The blots were visualized with the SuperSignal™ West Femto Maximum Sensitivity Substrate (Thermo Fisher Scientific).

Statistical Analysis

All data were presented as mean ± standard error of the means (SEM). Comparisons between groups were analyzed by unpaired two-tailed Student's *t*-test or two-way ANOVA. Statistical analysis was performed using Prism 6 (GraphPad). * $P < 0.05$; ** $P < 0.01$; *** $P < 0.001$; **** $P < 0.0001$.

Data and Software Availability

Next-generation sequencing data have been deposited in Gene Expression Omnibus (GEO) under SuperSeries accession code GEO: GSE110707, which includes individual data sets GEO: GSE110629 (RNA-seq; LM), GEO: GSE110706 (RNA-seq; VSV) and GEO: GSE110876 (ATAC-seq).

Supplementary Material

Refer to Web version on PubMed Central for supplementary material.

ACKNOWLEDGEMENTS

We thank J. Alderman, C. Lieber, E. Hughes-Picard and P. Musco for administrative assistance, J. Stein, L. Evangelisti and C. Hughes for generating *Klrg1*^{Cre} mice, Y. Harada and L. Yun-Cai for providing Foxo1-CA cDNA, S. Fujii for providing B16-OVA, P. Ranney, G. Lyon, Z. Tobiasova and L. Borelli for technical assistance, and members of the Flavell and Okada lab for helpful discussions. This work was supported by an Erwin Schrödinger Fellowship (Austrian Science Fund; J3220-B19 to D.H.B.), the Ministry of Education, Culture, Sports, Science, and Technology (16K19166 to H.I., 22113006 to T.O., and 26221306, 21229007 to T.K.), an Austrian Marshall Plan Foundation Fellowship (V.P.), a University of Vienna KWA Scholarship (C.S.), NIH grant 1R01HG008383–01A1 (Y.K.), Japan Science and Technology Agency (CREST J098501018 to T.K., and PRESTO to T.O.), and the Howard Hughes Medical Institute (R.A.F.).

REFERENCES

Anderson KG, Mayer-Barber K, Sung H, Beura L, James BR, Taylor JJ, Qunaj L, Griffith TS, Vezys V, Barber DL, and Masopust D (2014). Intravascular staining for discrimination of vascular and tissue leukocytes. Nat Protoc 9, 209–222. [PubMed: 24385150]

Araki K, Turner AP, Shaffer VO, Gangappa S, Keller SA, Bachmann MF, Larsen CP, and Ahmed R (2009). mTOR regulates memory CD8 T-cell differentiation. Nature 460, 108–112. [PubMed: 19543266]

Bergsbaken T, and Bevan MJ (2015). Proinflammatory microenvironments within the intestine regulate the differentiation of tissue-resident CD8$^+$ T cells responding to infection. Nat Immunol 16, 406–414. [PubMed: 25706747]

Best JA, Blair DA, Knell J, Yang E, Mayya V, Doedens A, Dustin ML, Goldrath AW, and Immunological Genome Project C (2013). Transcriptional insights into the CD8$^+$ T cell response to infection and memory T cell formation. Nat Immunol 14, 404–412. [PubMed: 23396170]

Bottcher JP, Beyer M, Meissner F, Abdullah Z, Sander J, Hochst B, Eickhoff S, Rieckmann JC, Russo C, Bauer T, et al. (2015). Functional classification of memory $CD8^+$ T cells by CX_3CR1 expression. Nat Commun 6, 8306. [PubMed: 26404698]

Buchholz VR, Schumacher TN, and Busch DH (2016). T Cell Fate at the Single-Cell Level. Annu Rev Immunol 34, 65–92. [PubMed: 26666651]

Buenrostro JD, Giresi PG, Zaba LC, Chang HY, and Greenleaf WJ (2013). Transposition of native chromatin for fast and sensitive epigenomic profiling of open chromatin, DNA-binding proteins and nucleosome position. Nat Methods 10, 1213–1218. [PubMed: 24097267]

Buenrostro JD, Wu B, Chang HY, and Greenleaf WJ (2015). ATAC-seq: A Method for Assaying Chromatin Accessibility Genome-Wide. Curr Protoc Mol Biol 109, 21 29 21–29.

Chang JT, Wherry EJ, and Goldrath AW (2014). Molecular regulation of effector and memory T cell differentiation. Nat Immunol 15, 1104–1115. [PubMed: 25396352]

Chen H, and Boutros PC (2011). VennDiagram: a package for the generation of highly-customizable Venn and Euler diagrams in R. BMC Bioinformatics 12, 35. [PubMed: 21269502]

Chu T, Tyznik AJ, Roepke S, Berkley AM, Woodward-Davis A, Pattacini L, Bevan MJ, Zehn D, and Prlic M (2013). Bystander-activated memory CD8 T cells control early pathogen load in an innate-like, NKG2D-dependent manner. Cell Rep 3, 701–708. [PubMed: 23523350]

Dominguez CX, Amezquita RA, Guan T, Marshall HD, Joshi NS, Kleinstein SH, and Kaech SM (2015). The transcription factors ZEB2 and T-bet cooperate to program cytotoxic T cell terminal differentiation in response to LCMV viral infection. J Exp Med 212, 2041–2056. [PubMed: 26503446]

Endrizzi BT, and Jameson SC (2003). Differential role for IL-7 in inducing lung Kruppel-like factor (Kruppel-like factor 2) expression by naive versus activated T cells. Int Immunol 15, 1341–1348. [PubMed: 14565932]

Falo LD Jr., Kovacsovics-Bankowski M, Thompson K, and Rock KL (1995). Targeting antigen into the phagocytic pathway in vivo induces protective tumour immunity. Nat Med 1, 649–653. [PubMed: 7585145]

Fernandez-Ruiz D, Ng WY, Holz LE, Ma JZ, Zaid A, Wong YC, Lau LS, Mollard V, Cozijnsen A, Collins N, et al. (2016). Liver-Resident Memory $CD8^+$ T Cells Form a Front-Line Defense against Malaria Liver-Stage Infection. Immunity 45, 889–902. [PubMed: 27692609]

Gerlach C, Moseman EA, Loughhead SM, Alvarez D, Zwijnenburg AJ, Waanders L, Garg R, de la Torre JC, and von Andrian UH (2016). The Chemokine Receptor CX3CR1 Defines Three Antigen-Experienced CD8 T Cell Subsets with Distinct Roles in Immune Surveillance and Homeostasis. Immunity 45, 1270–1284. [PubMed: 27939671]

Gray SM, Amezquita RA, Guan T, Kleinstein SH, and Kaech SM (2017). Polycomb Repressive Complex 2-Mediated Chromatin Repression Guides Effector $CD8^+$ T Cell Terminal Differentiation and Loss of Multipotency. Immunity 46, 596–608. [PubMed: 28410989]

Hara T, Shitara S, Imai K, Miyachi H, Kitano S, Yao H, Tani-ichi S, and Ikuta K (2012). Identification of IL-7-producing cells in primary and secondary lymphoid organs using IL-7-GFP knock-in mice. J Immunol 189, 1577–1584. [PubMed: 22786774]

Harada Y, Harada Y, Elly C, Ying G, Paik JH, DePinho RA, and Liu YC (2010). Transcription factors Foxo3a and Foxo1 couple the E3 ligase Cbl-b to the induction of Foxp3 expression in induced regulatory T cells. J Exp Med 207, 1381–1391. [PubMed: 20439537]

Hu G, and Chen J (2013). A genome-wide regulatory network identifies key transcription factors for memory $CD8^+$ T-cell development. Nat Commun 4, 2830. [PubMed: 24335726]

Jameson SC, and Masopust D (2009). Diversity in T cell memory: an embarrassment of riches. Immunity 31, 859–871. [PubMed: 20064446]

Joshi NS, Cui W, Chandele A, Lee HK, Urso DR, Hagman J, Gapin L, and Kaech SM (2007). Inflammation directs memory precursor and short-lived effector $CD8^+$ T cell fates via the graded expression of T-bet transcription factor. Immunity 27, 281–295. [PubMed: 17723218]

Jung YW, Rutishauser RL, Joshi NS, Haberman AM, and Kaech SM (2010). Differential localization of effector and memory CD8 T cell subsets in lymphoid organs during acute viral infection. J Immunol 185, 5315–5325. [PubMed: 20921525]

Kaech SM, and Cui W (2012). Transcriptional control of effector and memory CD8$^+$ T cell differentiation. Nat Rev Immunol 12, 749–761. [PubMed: 23080391]

Kaech SM, and Wherry EJ (2007). Heterogeneity and cell-fate decisions in effector and memory CD8$^+$ T cell differentiation during viral infection. Immunity 27, 393–405. [PubMed: 17892848]

Kanki H, Suzuki H, and Itohara S (2006). High-efficiency CAG-FLPe deleter mice in C57BL/6J background. Exp Anim 55, 137–141. [PubMed: 16651697]

Kim D, Pertea G, Trapnell C, Pimentel H, Kelley R, and Salzberg SL (2013). TopHat2: accurate alignment of transcriptomes in the presence of insertions, deletions and gene fusions. Genome Biol 14, R36. [PubMed: 23618408]

Kim SK, Schluns KS, and Lefrancois L (1999). Induction and visualization of mucosal memory CD8 T cells following systemic virus infection. J Immunol 163, 4125–4132. [PubMed: 10510347]

Klebanoff CA, Gattinoni L, Torabi-Parizi P, Kerstann K, Cardones AR, Finkelstein SE, Palmer DC, Antony PA, Hwang ST, Rosenberg SA, et al. (2005). Central memory self/tumor-reactive CD8$^+$ T cells confer superior antitumor immunity compared with effector memory T cells. Proc Natl Acad Sci U S A 102, 9571–9576. [PubMed: 15980149]

Kometani K, Nakagawa R, Shinnakasu R, Kaji T, Rybouchkin A, Moriyama S, Furukawa K, Koseki H, Takemori T, and Kurosaki T (2013). Repression of the transcription factor Bach2 contributes to predisposition of IgG1 memory B cells toward plasma cell differentiation. Immunity 39, 136–147. [PubMed: 23850379]

Kuwahara M, Ise W, Ochi M, Suzuki J, Kometani K, Maruyama S, Izumoto M, Matsumoto A, Takemori N, Takemori A, et al. (2016). Bach2-Batf interactions control Th2-type immune response by regulating the IL-4 amplification loop. Nat Commun 7, 12596. [PubMed: 27581382]

Langmead B, and Salzberg SL (2012). Fast gapped-read alignment with Bowtie 2. Nat Methods 9, 357–359. [PubMed: 22388286]

Mackay LK, and Kallies A (2017). Transcriptional Regulation of Tissue-Resident Lymphocytes. Trends Immunol 38, 94–103. [PubMed: 27939451]

Mackay LK, Rahimpour A, Ma JZ, Collins N, Stock AT, Hafon ML, Vega-Ramos J, Lauzurica P, Mueller SN, Stefanovic T, et al. (2013). The developmental pathway for CD103$^+$CD8$^+$ tissue-resident memory T cells of skin. Nat Immunol 14, 1294–1301. [PubMed: 24162776]

Martin M (2011). Cutadapt removes adapter sequences from high-throughput sequencing reads. EMBnet.journal 171, pp-10.

Mortier E, Advincula R, Kim L, Chmura S, Barrera J, Reizis B, Malynn BA, and Ma A (2009). Macrophage- and dendritic-cell-derived interleukin-15 receptor alpha supports homeostasis of distinct CD8$^+$ T cell subsets. Immunity 31, 811–822. [PubMed: 19913445]

Mueller SN, Gebhardt T, Carbone FR, and Heath WR (2013). Memory T cell subsets, migration patterns, and tissue residence. Annu Rev Immunol 31, 137–161. [PubMed: 23215646]

Obar JJ, and Lefrancois L (2010). Early signals during CD8 T cell priming regulate the generation of central memory cells. J Immunol 185, 263–272. [PubMed: 20519649]

Olson JA, McDonald-Hyman C, Jameson SC, and Hamilton SE (2013). Effector-like CD8$^+$ T cells in the memory population mediate potent protective immunity. Immunity 38, 1250–1260. [PubMed: 23746652]

Pearce EL, Walsh MC, Cejas PJ, Harms GM, Shen H, Wang LS, Jones RG, and Choi Y (2009). Enhancing CD8 T-cell memory by modulating fatty acid metabolism. Nature 460, 103–107. [PubMed: 19494812]

Pillai PS, Molony RD, Martinod K, Dong H, Pang IK, Tal MC, Solis AG, Bielecki P, Mohanty S, Trentalange M, et al. (2016). Mx1 reveals innate pathways to antiviral resistance and lethal influenza disease. Science 352, 463–466. [PubMed: 27102485]

Plumlee CR, Obar JJ, Colpitts SL, Jellison ER, Haining WN, Lefrancois L, and Khanna KM (2015). Early Effector CD8 T Cells Display Plasticity in Populating the Short-Lived Effector and Memory-Precursor Pools Following Bacterial or Viral Infection. Sci Rep 5, 12264. [PubMed: 26191658]

Pope C, Kim SK, Marzo A, Masopust D, Williams K, Jiang J, Shen H, and Lefrancois L (2001). Organ-specific regulation of the CD8 T cell response to Listeria monocytogenes infection. J Immunol 166, 3402–3409. [PubMed: 11207297]

Quinlan AR, and Hall IM (2010). BEDTools: a flexible suite of utilities for comparing genomic features. Bioinformatics 26, 841–842. [PubMed: 20110278]

Robinson JT, Thorvaldsdottir H, Winckler W, Guttman M, Lander ES, Getz G, and Mesirov JP (2011). Integrative genomics viewer. Nature biotechnology 29, 24–26.

Roychoudhuri R, Clever D, Li P, Wakabayashi Y, Quinn KM, Klebanoff CA, Ji Y, Sukumar M, Eil RL, Yu Z, et al. (2016). BACH2 regulates $CD8^+$ T cell differentiation by controlling access of AP-1 factors to enhancers. Nat Immunol 17, 851–860. [PubMed: 27158840]

Sarkar S, Kalia V, Haining WN, Konieczny BT, Subramaniam S, and Ahmed R (2008). Functional and genomic profiling of effector CD8 T cell subsets with distinct memory fates. J Exp Med 205, 625–640. [PubMed: 18316415]

Scott-Browne JP, Lopez-Moyado IF, Trifari S, Wong V, Chavez L, Rao A, and Pereira RM (2016). Dynamic Changes in Chromatin Accessibility Occur in $CD8^+$ T Cells Responding to Viral Infection. Immunity 45, 1327–1340. [PubMed: 27939672]

Sheridan BS, Pham QM, Lee YT, Cauley LS, Puddington L, and Lefrancois L (2014). Oral infection drives a distinct population of intestinal resident memory $CD8^+$ T cells with enhanced protective function. Immunity 40, 747–757. [PubMed: 24792910]

Shin H, and Iwasaki A (2012). A vaccine strategy that protects against genital herpes by establishing local memory T cells. Nature 491, 463–467. [PubMed: 23075848]

Shinnakasu R, Inoue T, Kometani K, Moriyama S, Adachi Y, Nakayama M, Takahashi Y, Fukuyama H, Okada T, and Kurosaki T (2016). Regulated selection of germinal-center cells into the memory B cell compartment. Nat Immunol 17, 861–869. [PubMed: 27158841]

Soudja SM, Ruiz AL, Marie JC, and Lauvau G (2012). Inflammatory monocytes activate memory $CD8^+$ T and innate NK lymphocytes independent of cognate antigen during microbial pathogen invasion. Immunity 37, 549–562. [PubMed: 22940097]

Steinert EM, Schenkel JM, Fraser KA, Beura LK, Manlove LS, Igyarto BZ, Southern PJ, and Masopust D (2015). Quantifying Memory CD8 T Cells Reveals Regionalization of Immunosurveillance. Cell 161, 737–749. [PubMed: 25957682]

Tainaka K, Kubota SI, Suyama TQ, Susaki EA, Perrin D, Ukai-Tadenuma M, Ukai H, and Ueda HR (2014). Whole-body imaging with single-cell resolution by tissue decolorization. Cell 159, 911–924. [PubMed: 25417165]

Trapnell C, Williams BA, Pertea G, Mortazavi A, Kwan G, van Baren MJ, Salzberg SL, Wold BJ, and Pachter L (2010). Transcript assembly and quantification by RNA-Seq reveals unannotated transcripts and isoform switching during cell differentiation. Nature biotechnology 28, 511–515.

Wherry EJ, Teichgraber V, Becker TC, Masopust D, Kaech SM, Antia R, von Andrian UH, and Ahmed R (2003). Lineage relationship and protective immunity of memory CD8 T cell subsets. Nat Immunol 4, 225–234. [PubMed: 12563257]

Wickham H (2009). ggplot2: Elegant Graphics for Data Analysis. Springer-Verlag New York.

Williams MA, and Bevan MJ (2007). Effector and memory CTL differentiation. Annu Rev Immunol 25, 171–192. [PubMed: 17129182]

Xin A, Masson F, Liao Y, Preston S, Guan T, Gloury R, Olshansky M, Lin JX, Li P, Speed TP, et al. (2016). A molecular threshold for effector $CD8^+$ T cell differentiation controlled by transcription factors Blimp-1 and T-bet. Nat Immunol 17, 422–432. [PubMed: 26950239]

Yang CY, Best JA, Knell J, Yang E, Sheridan AD, Jesionek AK, Li HS, Rivera RR, Lind KC, D'Cruz LM, et al. (2011). The transcriptional regulators Id2 and Id3 control the formation of distinct memory $CD8^+$ T cell subsets. Nat Immunol 12, 1221–1229. [PubMed: 22057289]

Yu B, Zhang K, Milner JJ, Toma C, Chen R, Scott-Browne JP, Pereira RM, Crotty S, Chang JT, Pipkin ME, et al. (2017). Epigenetic landscapes reveal transcription factors that regulate $CD8^+$ T cell differentiation. Nat Immunol 18, 573–582. [PubMed: 28288100]

Zhang Y, Liu T, Meyer CA, Eeckhoute J, Johnson DS, Bernstein BE, Nusbaum C, Myers RM, Brown M, Li W, and Liu XS (2008). Model-based analysis of ChIP-Seq (MACS). Genome Biol 9, R137. [PubMed: 18798982]

HIGHLIGHTS

- KLRG1^{+} IL-7Rα^{+} effector cells lose KLRG1 and differentiate into exKLRG1 memory cells
- ExKLRG1 memory cells comprise CX3CR1^{+} circulating and CX3CR1^{-} tissue-resident cells
- ExKLRG1 memory cells mount highly effective anti-viral and anti-tumor responses
- *Bach2* promotes exKLRG1 memory CD8^{+} T cell development

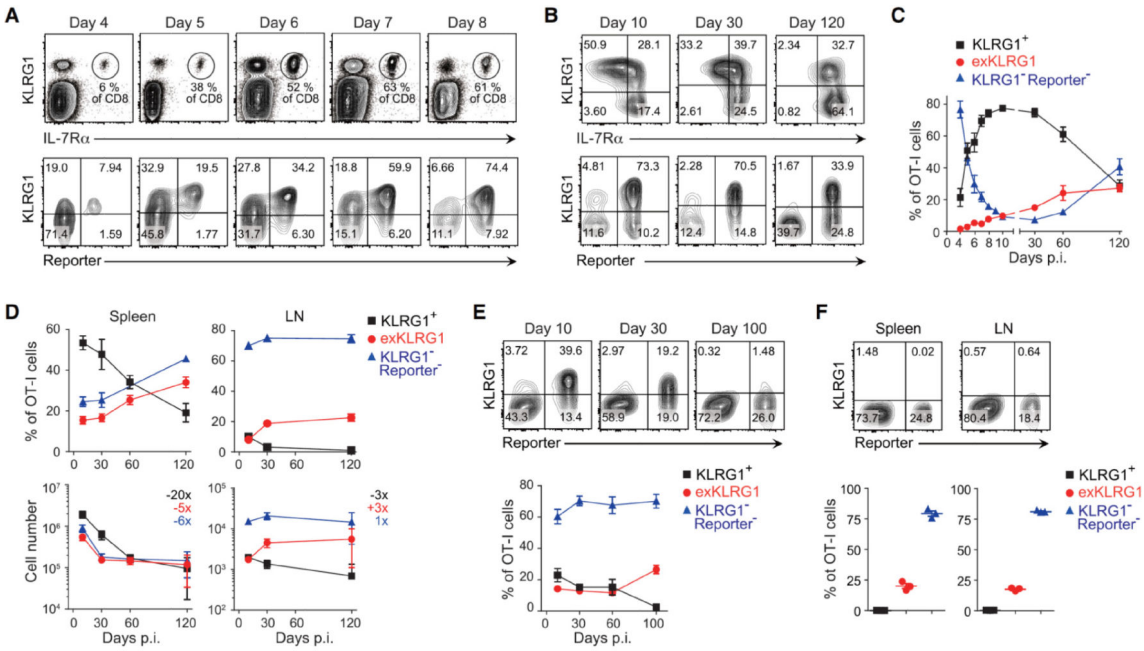

Figure 1. Effector CD8^{+} T Cells Lose KLRG1 Expression and Differentiate into Long-Lived Memory Cells.

(A and B) Expression of KLRG1 and fate mapping in effector OT-I cells in the blood following LM infection.

(C) Frequency of KLRG1^{+}, exKLRG1 and KLRG1^{-} Reporter^{-} cells among OT-I cells in the blood up to 120 days p.i. with LM.

(D) Percentage (top) and number (bottom) of OT-I cell subsets in the spleen and LN following LM infection. The numbers indicate fold difference in cell number between days 10 and 120.

(E) Frequency of KLRG1^{+}, exKLRG1 and KLRG1^{-} Reporter^{-} cells among OT-I cells in the blood up to 100 days p.i. with VSV.

(F) Percentage of KLRG1^{+}, exKLRG1 and KLRG1^{-} Reporter^{-} cells among OT-I cells in the spleen and LN 100 days p.i. with VSV.

Mean ± SEM are shown. Data are pooled from 2–4 independent experiments with 4–12 (C) or 3–12 mice per time point (D), or are representative of 2–3 independent experiments with 3–5 mice per time point (A, E, F). See also Figure S1 and S2.

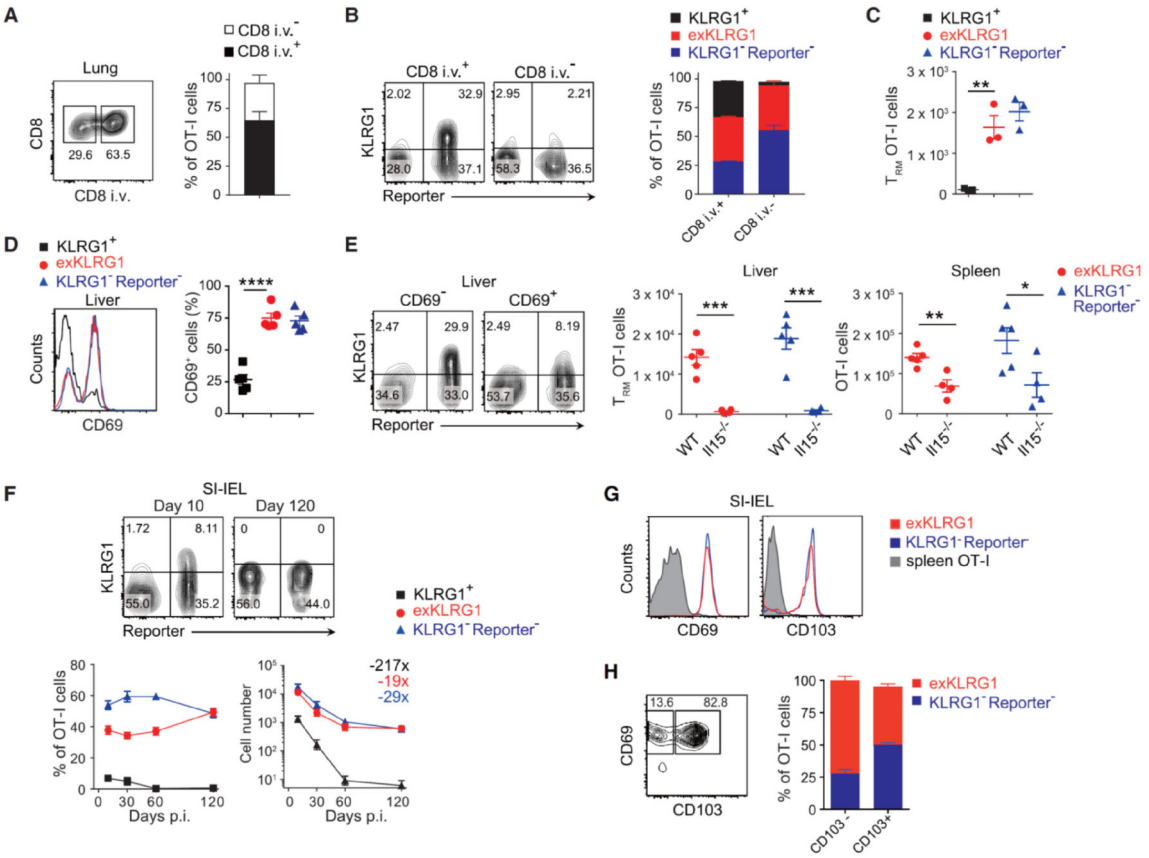

Figure 2. KLRG1^{+} Effector CD8^{+} T Cells Differentiate into Long-Lived Trm Cells.

(A-C) Frequency and number of resident (i.v.$^{-}$) and circulating (i.v.$^{+}$) memory OT-I cell subsets in the lung 60 days p.i. with LM. Circulating cells were identified by i.v. injection of anti-CD8α antibody.

(D) Frequency of CD69^{+} memory OT-I cell subsets in the liver 62 days p.i. with LM.

(E) Frequency and number of CD69^{+} Trm cells in the liver 30 days p.i. with LM.

(F) Frequency and number of OT-I cell subsets in the intraepithelial lymphocyte fraction of the small intestine (SI-IEL) 10 and 120 days p.i. with LM. Numbers indicate fold difference in cell number between days 10 and 120.

(G) Expression of CD69 and CD103 in OT-I cell subsets in the SI-IEL of mice orally infected with LM (day 42 p.i.).

(H) Frequency of CD103^{-} CD69^{+} or CD103^{+} CD69^{+} memory OT-I cell subsets in the SI-IEL.

Mean ± SEM are shown. ** $P < 0.01$, *** $P < 0.001$ and **** $P < 0.0001$ (unpaired two-tailed Student's *t*-test). Data are representative of two independent experiments with 3 (A-C), 4–5 (D, E), or 8 mice (G, H), or are pooled from 2–3 independent experiments with 4–9 mice per time point (F). See also Movies S1 and S2.

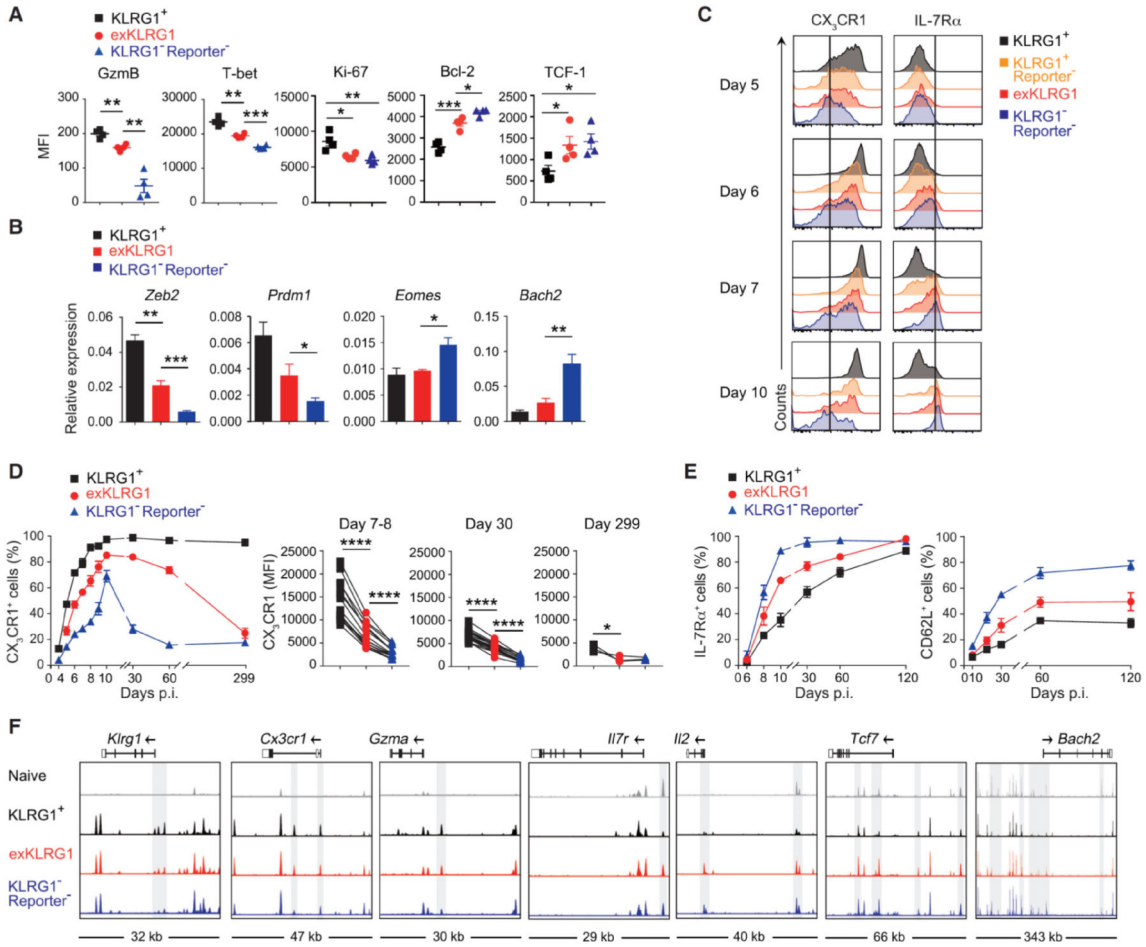

Figure 3. ExKLRG1 Effector CD8$^+$ T cells Express Cytotoxicity, Survival, and Proliferation Molecules at an Intermediate Level.

(A) Expression of GzmB, T-bet, Ki-67, Bcl-2, and TCF-1 in splenic effector OT-I cell subsets 9–10 days p.i. with LM.

(B) Expression of effector and memory signature genes in splenic OT-I cell subsets 8–11 days p.i. with LM.

(C-E) Time-dependent expression of CX_3CR1 and IL-7Rα in OT-I cell subsets in the blood following LM infection.

(F) Normalized ATAC-seq signal profiles across 7 gene loci in splenic naïve and effector OT-I cell subsets (8 days p.i. with LM). Peaks differentially expressed between OT-I cell subsets are highlighted in grey.

Mean ± SEM are shown. * $P < 0.05$, ** $P < 0.01$ and *** $P < 0.001$ (unpaired two-tailed Student's *t*-test). Data are representative of 2–3 independent experiments with 4–8 mice (A, C), pooled from 2–3 independent experiments with 3–11 mice per time point (B, D, E), or 2 independent experiments with pooled cells from 2–3 mice (F). See also Figure S3.

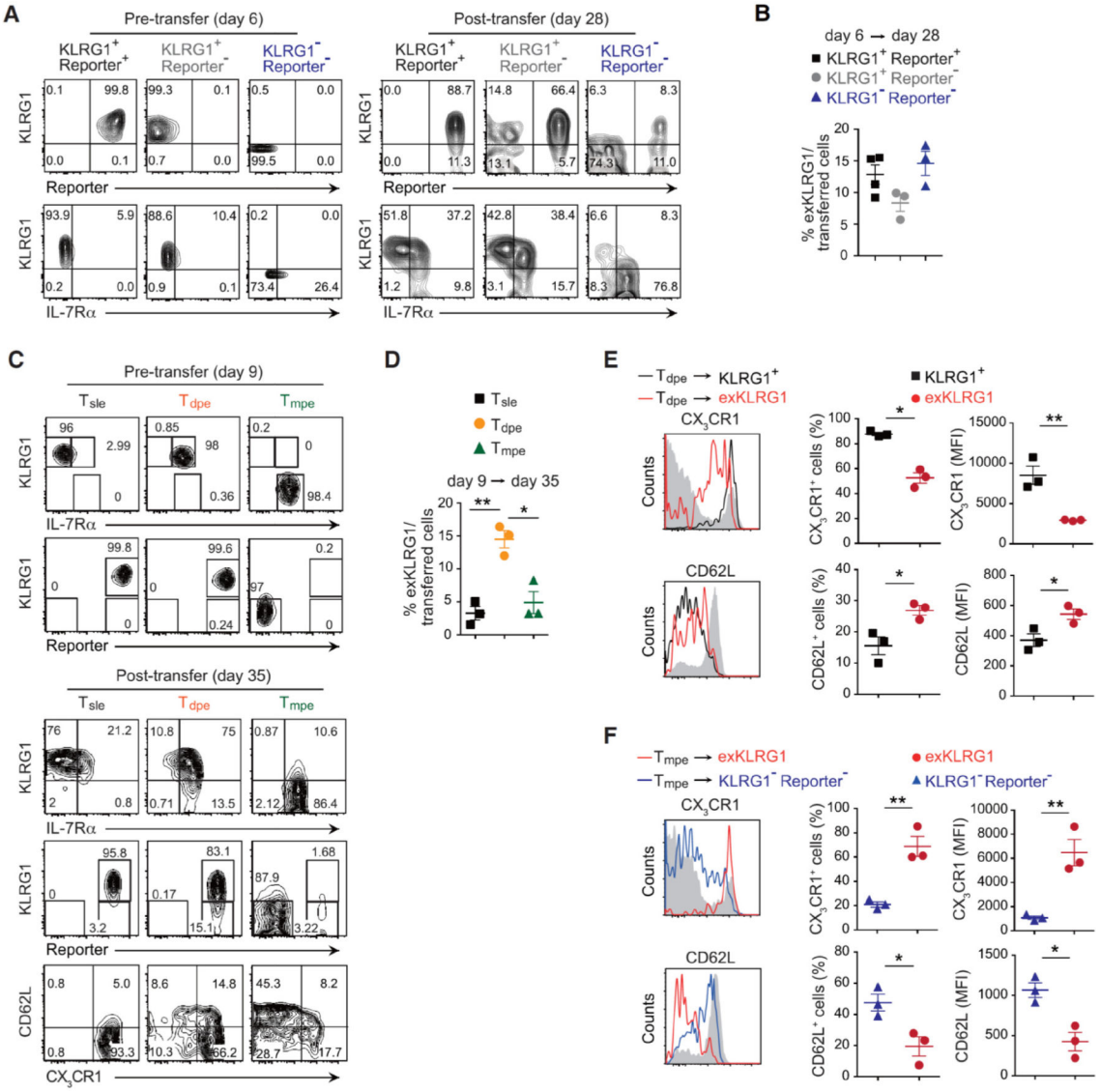

Figure 4. Developmental Plasticity of Effector CD8$^+$ T cell Subsets Following LM Infection.

(A) Expression of KLRG1, IL-7Rα and tdTomato in splenic effector OT-I cell subsets 6 days p.i. with LM (pre-transfer) and 22 days post-transfer (day 28 p.i.).

(B) Development of exKLRG1 memory cells (day 28 p.i.) from three different effector OT-I cell subsets 6 days p.i. with LM.

(C) Expression of KLRG1, IL-7Rα, tdTomato, CD62L and CX_3CR1 in splenic effector OT-I cell subsets 9 days p.i. with LM (pre-transfer) and 26 days post-transfer (day 35 p.i.).

(D) Development of exKLRG1 memory cells (day 35 p.i.) from three different effector OT-I cell subsets 9 days p.i. with LM.

(E) Expression of CX_3CR1 and CD62L in KLRG1$^+$ and exKLRG1 memory cells 26 days post transfer of day 9 Tdpe cells. Host CD8$^+$ T cells served as a control (gray line).

(F) Expression of CX_3CR1 and CD62L in exKLRG1 and KLRG1$^-$ Reporter$^-$ memory cells 26 days post transfer of day 9 Tmpe cells. Host CD8$^+$ T cells served as a control (gray line).

Mean ± SEM are shown. * $P < 0.05$ and ** $P < 0.01$ (unpaired two-tailed Student's *t*-test). Data are representative of two independent experiments with 3–4 mice. See also Figure S4.

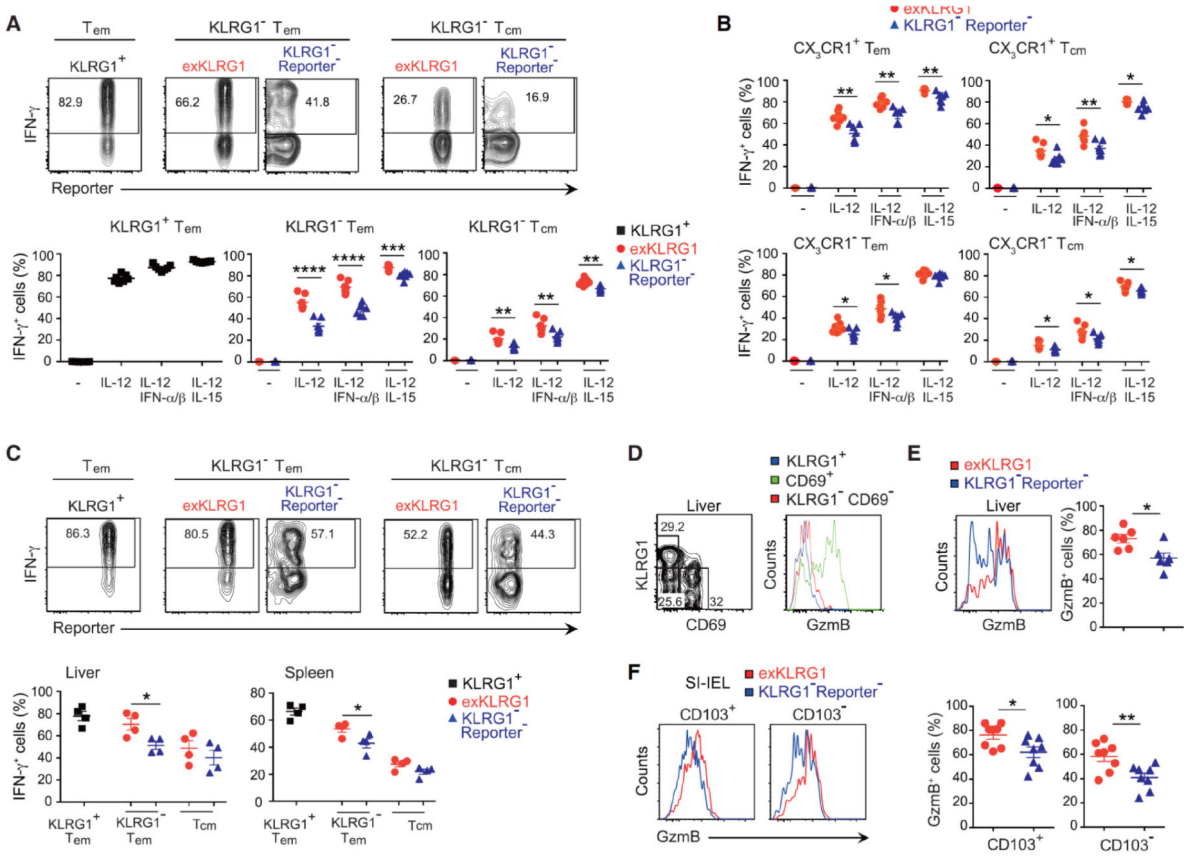

Figure 5. ExKLRG1 Memory Cell Subsets Retain High Cytotoxic Capacity and Responsiveness to IL-12.

(A and B) Production of IFN-γ in splenic Tem (KLRG1$^+$ CD62L$^-$ or KLRG1$^-$ CD62L$^-$) and Tcm (KLRG1$^-$ CD62L$^+$) OT-I cells (A) or Tem (KLRG1$^-$ CX$_3$CR1$^+$ CD62L$^-$) and Tcm (KLRG1$^-$ CX$_3$CR1$^+$ CD62L$^+$) OT-I cells (B) following stimulation with IL-12 (density plots), IL-12 + IFNα/β or IL-12 + IL-15 for 7 hours *in vitro*.

(C) Memory OT-I cells were generated as described in Figure S1E and mice were challenged 90 days later with *Listeria monocytogenes*, which did not express OVA. Production of IFN-γ in Tem (KLRG1$^+$ CD62L$^-$ or KLRG1$^-$ CD62L$^-$) and Tem (KLRG1$^-$ CD62L$^+$) OT-I cells in spleen and liver (density plots) 12 hours after rechallenge.

(D) Expression of GzmB in circulating memory (KLRG1$^+$CD69$^-$ or KLRG1$^-$CD69$^-$) and Trm (KLRG1$^-$CD69$^+$) cells within the endogenous OVA-tetramer$^+$ CD44^{hi} CD8$^+$ T cell population in the liver 108 days p.i. with LM.

(E) Expression of GzmB in KLRG1$^-$ Reporter$^-$ Trm and exKLRG1 tetramer$^+$ Trm cells in the liver 108 days p.i. with LM.

(F) Expression of GzmB in KLRG1$^-$ Reporter$^-$ Trm and exKLRG1 Trm cells within intraepithelial CD103$^+$ CD69$^+$ and CD103$^-$ CD69$^+$ OT-I cell subsets 42 days after oral infection with LM (n=8).

Mean ± SEM are shown. * $P < 0.05$, ** $P < 0.01$, *** $P < 0.001$ and **** $P < 0.0001$ (unpaired two-tailed Student's *t*-test). The data are representative of two (C-F) or three (A, B) independent experiment with 3–7 mice. See also Figure S5.

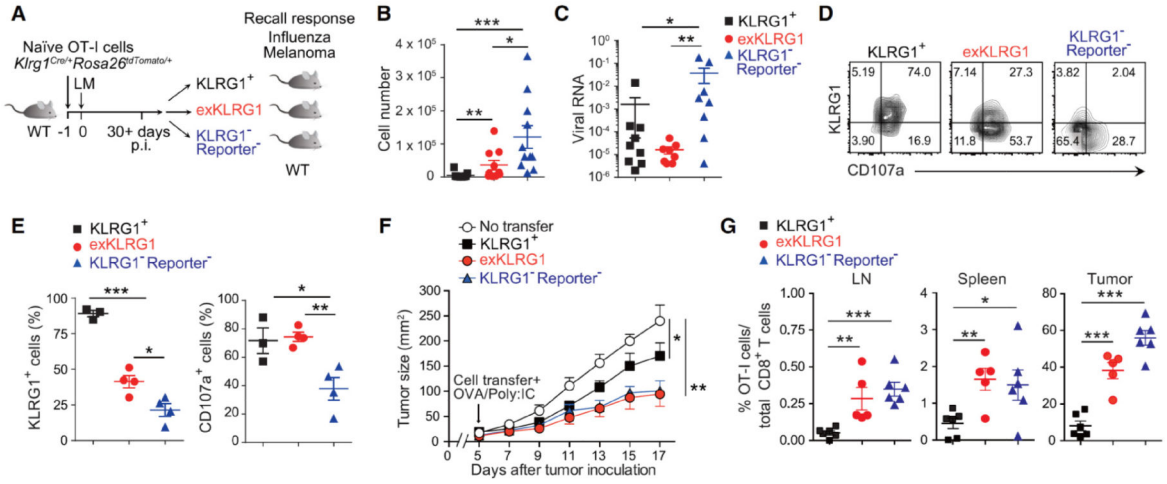

Figure 6. ExKLRG1 Memory CD8$^+$ T cells Mount Potent Anti-Influenza and Anti-Tumor Responses.

(A) Schematic of the adoptive transfer and infection experiments.

(B) Mice receiving memory OT-I cell subsets were challenged i.n. with OVA-expressing influenza virus (FLU). Seven days later, the number of effector OT-I cells in the lung was determined.

(C) Viral RNA in the lung 7 days p.i. with FLU was determined by quantitative RT-PCR.

(D and E) Expression of KLRG1 and CD107a in effector OT-I cell subsets in the lung 7 days p.i. with FLU.

(F) Tumor size of mice s.c. injected with melanoma cells (B16-OVA) followed by adoptive transfer of memory OT-I cell subsets.

(G) Percentage of transferred OT-I cells within total CD8$^+$ T cells in the LN, spleen and tumor at day 17 after tumor inoculation.

Data were analyzed by unpaired two-tailed Student's *t*-test (B, C, E) or two-way ANOVA (F). Mean ± SEM are shown. * $P < 0.05$, ** $P < 0.01$ and *** $P < 0.001$. Data are pooled from 2–3 experiments with 10–11 mice (B and C), or representative of two (D, E) or three (F, G) independent experiments with 3–4 (D, E) and 5–6 (F, G) mice.

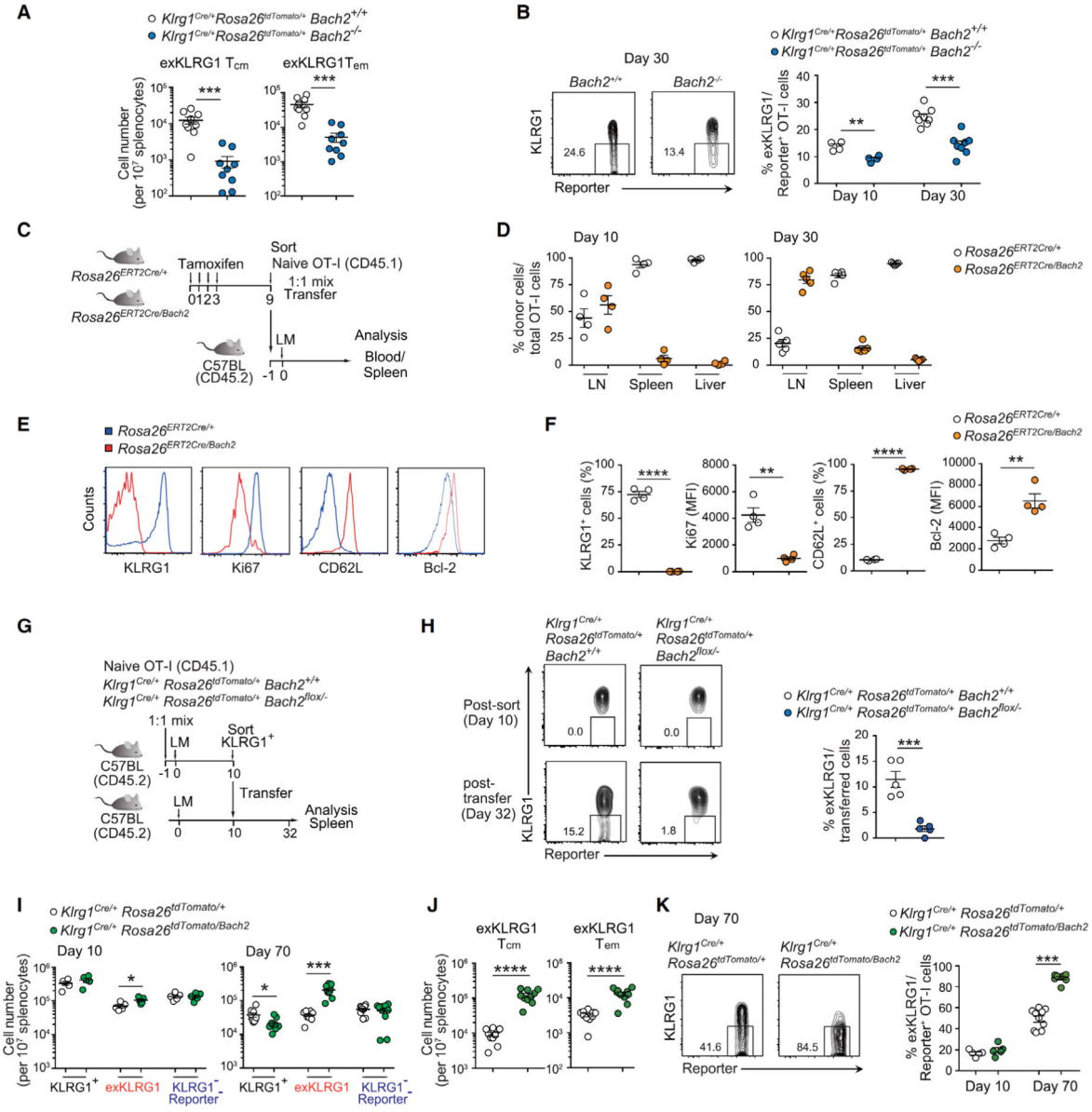

Figure 7. Bach2 Supports the Differentiation of KLRG1$^+$ Effector Cells into ExKLRG1 Memory Cells.

(A) Naive *Klrg1*$^{Cre/+}$*Rosa26*$^{tdTomato/+}$*Bach2*$^{+/+}$ and *Klrg1*$^{Cre/+}$*Rosa26*$^{tdTomato/+}$*Bach2*$^{-/-}$ OT-I cells from different CD45 congenic backgrounds were co-transferred into WT mice, followed by infection with LM one day later. The number of exKLRG1 Tcm and exKLRG1 Tem OT-I cells in the spleen 30 days p.i. with LM is shown.

(B) Percentage of exKLRG1 cells among Reporter$^+$ donor OT-I cells in the spleen 10 and 30 days p.i. with LM.

(C) Schematic of the experimental protocol for (D-F). Tamoxifen was injected for four consecutive days to induce Cre-dependent Bach2 expression in OT-I *Rosa26*$^{ERT2Cre/Bach2}$ mice. After 9 days, Bach2-expressed GFP$^+$ naïve OT-I cells were sorted, mixed with *Rosa26*$^{ERT2Cre/+}$ *naïve* OT-I cells at a 1:1 ratio, and transferred into C57BL/6 mice followed by infection with LM one day later.

(D) Relative frequency of *Rosa26*$^{ERT2Cre/+}$ and *Rosa26*$^{ERT2Cre/Bach}$ OT-I cells 10 and 30 days p.i. with LM in the LN, spleen and liver.
(E and F) Expression of CD62L, KLRG1, Ki-67 and Bcl-2 in *Rosa26*$^{ERT2Cre/+}$ and *Rosa26*$^{ERT2Cre/Bach}$ OT-I cells 10 days p.i. with LM.
(G) Schematic of the experimental protocol for (H).
(H) Expression of KLRG1 and Reporter in OT-I cells post-transfer of day 10 KLRG1^{+} effector OT-I cells into infection-matched WT mice (32 days p.i. with LM).
(I) Naive *Klrg1*$^{Cre/+}$*Rosa26*$^{tdTomato/+}$ and *Klrg1*$^{Cre/+}$*Rosa26*$^{tdTomato/Bach2}$ OT-I cells from different CD45 congenic backgrounds were co-transferred into WT mice, followed by infection with LM one day later. The number of KLRG1^{+}, exKLRG1 and KLRG1^{-}Reporter^{-} OT-I cells in the spleen at days 10 and 70 p.i. with LM is shown.
(J) Percentage of exKLRG1 cells among Reporter^{+} OT-I cells in the spleen 70 days p.i. with LM.
(K) Number of exKLRG1 Tcm and exKLRG1 Tem OT-I cells in the spleen 70 days p.i. with LM.
Mean ± SEM are shown. * $P < 0.05$, ** $P < 0.01$, *** $P < 0.001$, **** $P < 0.0001$ (unpaired two-tailed Student's *t*-test). Data are representative of two independent experiments with 5 (D-H) or 4–10 (A, B, I-K) mice. See also Figure S5, S6, and S7.

KEY RESOURCES TABLE

REAGENT or RESOURCE	SOURCE	IDENTIFIER
Antibodies		
Anti-mouse Bcl2 (BCL/10C4) AF647	BioLegend	Cat#633509, RRID:AB_2064149
Anti-mouse B220 (RA3–6B2) BV510	BioLegend	Cat#103247, RRID:AB_2561394
Anti-mouse B220 (RA3–6B2) Biotin	BioLegend	Cat#103204, RRID:AB_312989
Anti-mouse CCR7 (4B12) Biotin	BioLegend	Cat#120104, RRID:AB_389232
Anti-mouse CD4 (RM4–5) FITC	BD Biosciences	Cat#553047, RRID:AB_394583
Anti-mouse CD4 (RM4–5) Biotin	BioLegend	Cat#100508, RRID:AB_312711
Anti-mouse CD4 (RM4–5) APC-Cy7	BioLegend	Cat#100526, RRID:AB_312727
Anti-mouse CD8α (53–6.7) PE	BioLegend	Cat#100708, RRID:AB_312747
Anti-mouse CD8α (53–6.7) PE-Cy7	BioLegend	Cat#100722, RRID:AB_312761
Anti-mouse CD8α (53–6.7) BV510	BioLegend	Cat#100752, RRID:AB_2563057
Anti-mouse CD8α (53–6.7) PerCP	Biolegend	Cat#100732, RRID:AB_893423
Anti-mouse CD8α (53–6.7) APC-Cy7	BioLegend	Cat#100714, RRID:AB_312753
Anti-mouse CD8α (53–6.7) Pacific Blue	BD Biosciences	Cat#558106, RRID:AB_397029
Anti-mouse CD11b (M1/70) V500	BD Biosciences	Cat#562127, RRID:AB_10893815
Anti-mouse CD11b (M1/70) Biotin	BioLegend	Cat#101204, RRID:AB_312787
Anti-mouse CD11c (N418) PE-Cy7	Thermo Fisher Scientific	Cat#25–0114-82, RRID:AB_469590
Anti-mouse CD11c (N418) Biotin	BioLegend	Cat#117304, RRID:AB_313773
Anti-mouse CD43 (1B11) PE-Cy7	BioLegend	Cat#121218, RRID:AB_528813
Anti-mouse CD44 (IM7) V500	BD Biosciences	Cat#560781, RRID:AB_1937328
Anti-mouse CD44 (IM7) FITC	BioLegend	Cat#103022, RRID:AB_493685
Anti-mouse CD44 (IM7) APC-Cy7	BioLegend	Cat#103028, RRID:AB_830785
Anti-mouse CD45.1 (A20) FITC	Thermo Fisher Scientific	Cat#11–0453-82, RRID:AB_465058
Anti-mouse CD45.1 (A20) PE-Cy7	BioLegend	Cat#110730, RRID:AB_1134168
Anti-mouse CD45.1 (A20) Pacific Blue	BioLegend	Cat#110722, RRID:AB_492866
Anti-mouse CD45.1 (A20) AF700	BioLegend	Cat#110724, RRID:AB_493733
Anti-mouse CD45.2 (104) FITC	BD Biosciences	Cat#553772, RRID:AB_395041
Anti-mouse CD62L (MEL-14) APC-Cy7	BioLegend	Cat#104428, RRID:AB_830799

REAGENT or RESOURCE	SOURCE	IDENTIFIER
Anti-mouse CD62L (MEL-14) eFluor450	Thermo Fisher Scientific	Cat#48–0621-82, RRID:AB_1963590
Anti-mouse CD69 (H1.2F3) FITC	BioLegend	Cat#104506, RRID:AB_313109
Anti-mouse CD69 (H1.2F3) PE-Cy7	BD Biosciences	Cat#552879, RRID:AB_394508
Anti-mouse CD69 (H1.2F3) Pacific Blue	BioLegend	Cat#104524, RRID:AB_2074979
Anti-mouse CD103 (2E7) FITC	BioLegend	Cat#121420, RRID:AB_10714791
Anti-mouse CD103 (2E7) Pacific Blue	BioLegend	Cat#121418, RRID:AB_2128619
Anti-mouse CD107a (1D4B) AF488	BioLegend	Cat#121608, RRID:AB_571983
Anti-mouse CD127 (SB/199) APC	BD Biosciences	Cat#564175
Anti-mouse CD127 (SB/199) BV711	BD Biosciences	Cat#565490
Anti-mouse CD127 (A7R34) eFluor450	Thermo Fisher Scientific	Cat#48–1271-80, RRID:AB_2016629
Anti-mouse CD127 (A7R34) Biotin	Thermo Fisher Scientific	Cat#13–1271-85, RRID:AB_466589
Anti-mouse CXCR3 (173) PE-Cy7	BioLegend	Cat#126516, RRID:AB_2245493
Anti-mouse CX3CR1 (SA011F11) FITC	BioLegend	Cat#149020, RRID:AB_2565703
Anti-mouse CX3CR1 (SA011F11) PE-Cy7	BioLegend	Cat#149016, RRID:AB_2565700
Anti-mouse CX3CR1 (SA011F11) Biotin	BioLegend	Cat#149018, RRID:AB_2565701
Anti-mouse Eomes (Dan11mag) eFluor450	Thermo Fisher Scientific	Cat#48–4875-80, RRID:AB_2574061
Anti-mouse FLAG (DYKDDDDK) (L5) PE	BioLegend	Cat#637309, RRID:AB_2563147
Anti-mouse Foxp3 (FJK-16s) APC	Thermo Fisher Scientific	Cat#17–5773-82, RRID:AB_469457
Anti-mouse Gr1 (RB6–8C5) APC	BioLegend	Cat#108412, RRID:AB_313377
Anti-mouse Gr1 (RB6–8C5) Biotin	BioLegend	Cat#108404, RRID:AB_313369
Anti-mouse Granzyme B (GB11) AF647	BioLegend	Cat#515405, RRID:AB_2294995
Anti-mouse IFN-γ (XMG1.2) APC	BioLegend	Cat#505810, RRID:AB_315404
Anti-mouse IL-2 (JES6–5H4)	BioLegend	Cat#503831, RRID:AB_2561749
Anti-mouse Ki-67 (16A8) APC	BioLegend	Cat#652405, RRID:AB_2561929
Anti-mouse Ki-67 (B56) AF647	BD Biosciences	Cat#561126, RRID:AB_10611874
Anti-mouse KLRG1 (2F1) FITC	BioLegend	Cat#138409, RRID:AB_10643998
Anti-mouse KLRG1 (2F1) PE-Cy7	BioLegend	Cat#138416, RRID:AB_2561736
Anti-mouse KLRG1 (2F1) BV421	BioLegend	Cat#138414, RRID:AB_2565613
Anti-mouse KLRG1 (2F1) APC	BioLegend	Cat#138412, RRID:AB_10641560

REAGENT or RESOURCE	SOURCE	IDENTIFIER
Anti-mouse KLRG1 (2F1) APC	Thermo Fisher Scientific	Cat#17–5893-82, RRID:AB_469469
Anti-mouse NK1.1 (PK136) FITC	BioLegend	Cat#108705, RRID:AB_313392
Anti-mouse T-bet (4B10) APC	BioLegend	Cat#644813, RRID:AB_10896913
Anti-mouse TCF1 (C63D9) AF647	Cell Signaling Technology	Cat#6709
Anti-RFP	Rockland	Cat#600–401-379, RRID:AB_2209751
Anti-RFP biotin	Rockland	Cat#600–406-379, RRID:AB_828390
Anti-rabbit AF594	Thermo Fisher Scientific	Cat#R37117, RRID:AB_2556545
Anti-mouse FLAG (M2)	Sigma-Aldrich	Cat#F1804, RRID:AB_262044
Anti-mouse Actin (C-11)	Santa Cruz Biotechnology	Cat#sc-1615, RRID:AB_630835
Anti-mouse Bach2	Abcam	Cat#ab83364, RRID:AB_1861444
Bacterial and Virus Strains		
Listeria monocytogenes (EGD)	Yoshikai Y (Kyushu University)	N/A
Listeria monocytogenes expressing OVA	Shen H (University of Pennsylvania) Pope C et al., 2001	N/A
Vesicular stomatitis virus expressing OVA	Kim et al., 1999	N/A
Influenza A/PR8 virus expressing OVA	Iwasaki A (Yale University), Garcia-Sastre A (Icahn School of Medicine at Mount Sinai)	N/A
Biological Samples		
Chemicals, Peptides, and Recombinant Proteins		
T-Select H-2Kb OVA Tetramer-SIINFEKL-APC	MBL	Cat#TS-5001–2C
Rapamycin	Calbiochem	Cat#553210
Tamoxifen	Sigma-Aldrich	Cat#T5648
Sunflower seed oil	Sigma-Aldrich	Cat#S5007
OptiPrep	Axis-Shield	Cat#1114542
Percoll	GE Healthcare	Cat#17089101
Collagenase IV	Sigma-Aldrich	Cat#C5138
DNase I	Sigma-Aldrich	Cat#DN25
TRIzol™ Reagent	Thermo Fisher Scientific	Cat#15596018
Ovalbumin, Low Endo, Purified	Worthington Biochemical Corporation	Cat#LS003061
Poly(I)•Poly(C)	GE Healthcare	Cat#27473201
Foxo1 inhibitor	Calbiochem	Cat#AS1842856

REAGENT or RESOURCE	SOURCE	IDENTIFIER
OVA (257–264) SIINFEKL	AnaSpec	Cat#AS-60193–1
Protein Transport Inhibitor (containing Monensin)	BD Biosciences	Cat#554724
Brefeldin A Solution	BioLegend	Cat#420601
N,N,N',N'-Tetrakis(2hydroxypropyl)ethylenediamine	Tokyo Chemical Industry	Cat#T0781
Polyethylene glycol mono-p-isooctylphenyl ether (Triton X-100)	Nacalai Tesque	Cat#25987–85
Urea	Nacalai Tesque	Cat#35904–45
Dynabeads™ Mouse T-Activator CD3/CD28	Thermo Fisher Scientific	Cat#11452D
Recombinant mouse IL-2	R&D Systems	Cat#402-ML
Recombinant mouse IL-12	PeproTech	Cat#210–12
Recombinant mouse IL-15	PeproTech	Cat#210–15
Recombinant mouse IFN-α	PBL Assay Science	Cat#12100–1
Recombinant mouse IFN-β	PBL Assay Science	Cat#12400–1
PE Streptavidin	BioLegend	Cat#405204
APC Streptavidin	BioLegend	Cat#405207
Critical Commercial Assays		
eBioscience™ FoxP3/transcription factor buffer set	Thermo Fisher Scientific	Cat#00–5523-00
Fixation/Permeabilization Solution Kit	BD Biosciences	Cat#554714
Nuclear Extract Kit	Active Motif	Cat#40010
Streptavidin MicroBeads	Miltenyi Biotec	Cat#130–048-102
MojoSort™ Streptavidin Nanobeads	BioLegend	Cat#480016
EasySep™ Mouse Naive CD8+ T cell Isolation Kit	STEMCELL Technologies	Cat#19858A
RNeasy Mini Kit	Qiagen	Cat#74104
SureSelect Strand Specific RNA Library	Agilent	G9691A
Nextera DNA Library Preparation Kit	Illumina	Cat#FC-121–1030
Deposited Data		
Raw and processed data (RNA-seq and ATAC-seq)	This paper	GEO: GSE110707
Experimental Models: Cell Lines		
B16 melanoma expressing OVA	Fujii S (RIKEN) Falo DR et al., 1995	N/A
Experimental Models: Organisms/Strains		

REAGENT or RESOURCE	SOURCE	IDENTIFIER
Mouse: C57BL/6 (B6)	National Cancer Institute	N/A
Mouse: C57BL/6 (B6)	Charles River Laboratories	N/A
Mouse: C57BL/6 (B6)	CLEA Japan	N/A
Ly5.2/Cr (CD45.1)	National Cancer Institute	N/A
C57BL/6-Tg(TcraTcrb)1100Mjb/J	The Jackson Laboratory	JAX: 003831
C57BL/6-Tg(UBC-GFP)30Scha/J	The Jackson Laboratory	JAX: 004353
B6.129X1-*Gt(ROSA)26Sortm1(EYFP)Cos*/J	The Jackson Laboratory	JAX: 006148
B6.Cg-Gt(ROSA)26Sortm14(CAG-tdTomato)Hze/J	The Jackson Laboratory	JAX: 007914
B6.Cg-Tg(Pgk1-flpo)10Sykr/J	The Jackson Laboratory	JAX: 011065
C57BL/6-Tg(CAG-flpe)36Ito/ItoRbrc	RIKEN BioResource Center, Kanki et al., 2006	RBRC01834
B6.129S6-*Rag2tm1Fwa* N12	Taconic Biosciences	RAGN12
C57BL/6-*Gt(ROSA)26Sortm9(Cre/ESR1)Arte*	Taconic Biosciences	10471
Klrg1^{Cre}	This paper	N/A
Bach2^{Flag}	This paper	N/A
Bach2$^{flox/flox}$	Kometani et al., 2013	N/A
Rosa26^{Bach2}	Kuwahara et al., 2016	N/A
Oligonucleotides		
Primer for genotyping: Klrg1-Cre Common: TTTGCCCAGATTTAGGCTTT Klrg1-Cre: CTGTGTCTGGTGTGGCTGAT Wild-type: ATTCACAGAAATGGCCTCCA	This paper	N/A
Primer for genotyping: Bach2-Flag Forward: GCTCATGGGACCTGGGAGCTTTGG Reverse: CCGTTGGTCATTGAGGCCCAGGAGG	This paper	N/A
Primer for quantitative PCR: Bach2 deleted allele Forward flox: TGGCTCCCCCATGTATGTAT Reverse flox: ATCAGCGTCACGTCACAGAG Forward control: CCTAGGAAACTGGGATGACG Reverse control: GGGGTCTTCTTAAGGCCAAC	This paper	N/A
Primer for quantitative RT-PCR: Actb Forward: TTCTTTGCAGCTCCTTCGTT Reverse: ATGGAGGGGAATACAGCCC	This paper	N/A
Primer for quantitative RT-PCR: Bach2 Forward: CACTGGTTGGACAGACGAAA Reverse: ACTGTAGCAGTGGCCCAAAG	This paper	N/A

REAGENT or RESOURCE	SOURCE	IDENTIFIER
Primer for quantitative RT-PCR: Eomes Forward: ATGTACGTTCACCCAGAATC Reverse: GTGCAGAGACTGCAACACTA	Dominguez et al., 2015	N/A
Primer for quantitative RT-PCR: Gzma Forward: TCAGCTCCCTCTGAAACTCT Reverse: TCTCCACCAAAAGAGGTGAT	Dominguez et al., 2015	N/A
Primer for quantitative RT-PCR: iCre Forward: CACCTGGAAGATGCTCCTGT Reverse: TCCCTCACATCCTCAGGTTC	This paper	N/A
Primer for quantitative RT-PCR: Id3 Forward: ACTTACCCTGAACTCAACGC Reverse: CTCCAAGGAAACCAGAAGAA	Dominguez et al., 2015	N/A
Primer for quantitative RT-PCR: Influenza A/PR8/M Forward: CGCTCAGACATGAGAACAGAATGG Reverse: TAACTAGCCTGACTAGCAACCTC	Pillai et al., 2016	N/A
Primer for quantitative RT-PCR: Klf2 Forward: AGCCTATCTTGCCGTCCTT Reverse: CCAACACGTTGTTTAGGTCCTC	Endrizzi and Jameson, 2003	N/A
Primer for quantitative RT-PCR: Prdm1 Forward: ACCAAGGAACCTGCTTTTCA Reverse: GGCATTCTTGGGAACTGTGT	This paper	N/A
Primer for quantitative RT-PCR: S1pr5 Forward: GTACACCAAATGCCCAGCTT Reverse: CACTGGAGCACTGTGCAAAA	This paper	N/A
Primer for quantitative RT-PCR: Zeb2 Forward: AGAAGCCACGATCCAGACC Reverse: GGCCATCTCTTTCCTCCAGT	This paper	N/A
Recombinant DNA		
pMCs-Foxo1-CA-IRES-GFP	Liu YC (La Jolla Institute) Harada et al., 2010	N/A
Software and Algorithms		
BEDTools	Quinlan and Hall, 2010	N/A
Bowtie 2	Langmead and Salzberg, 2012	http://bowtiebio.sourceforge.net/bowtie2/index.shtml
Casava 1.8.2	Illumina	N/A
Cufflinks version 2.1.1	Trapnell et al., 2010	N/A
Cutadapt 1.8.3	Martin, 2011	N/A
FlowJo 9 and 10	Tree Star	https://www.flowjo.com/solutions/flowjo/downloads
GraphPad Prism 6.0	GraphPad	https://www.graphpad.com

REAGENT or RESOURCE	SOURCE	IDENTIFIER
Imaris 8	Bitplane	http://www.bitplane.com/download
MACS2	Zhang et al., 2008	N/A
Picard MarkDuplicate tool	N/A	http://broadinstitute.github.io/picard
R (for principal component analysis)	N/A	http://www.rproject.org/
TopHat2 version 2.0.8	Kim et al., 2013	N/A
VennDiagram package	Chen and Boutros, 2011	N/A